Geotechnique

Numerical and theoretical analyses of settlements of strip shallow foundations on normally-consolidated clays under partially drained conditions

--Manuscript Draft--

Manuscript Number:	19-P-348R2
Full Title:	Numerical and theoretical analyses of settlements of strip shallow foundations on normally-consolidated clays under partially drained conditions
Article Type:	General Paper
Corresponding Author:	Luca Flessati Politecnico di Milano Milan, ITALY
Corresponding Author's Institution:	Politecnico di Milano
Order of Authors:	Luca Flessati
	Claudio di Prisco
	Fabio Callea
Corresponding Author's Secondary Institution:	
Order of Authors Secondary Information:	
Manuscript Region of Origin:	ITALY
Abstract:	In the geotechnical community, the macroelement approach nowadays is largely considered to be a successful theoretical tool for solving soil-structure interaction problems. This approach is based on the definition of a generalized constitutive law putting in relation a small number of suitably defined generalized stress/strain variables. The macroelement formulations proposed in the literature take into consideration either drained or undrained cases, but disregard the hydro-mechanical coupling. In this paper, the authors intend to generalize the theory by introducing a new formulation for shallow foundations overpassing this limitation and capable of accounting for the influence of loading rate on the system response. To conceive and to calibrate the model, the authors numerically analysed the case of a shallow foundation positioned on a normally consolidated clayey soil stratum whose mechanical behaviour is reproduced by means of the Modified Cam Clay model. Finally, the approach is critically discussed in the perspective of its use as designing tool according to ultimate limit state and displacement based approaches.
Suggested Reviewers:	David Muir Wood University of Dundee d.muirwood@dundee.ac.uk For his experties in the field
	Guy Houlsby University of Oxford guy.houlsby@eng.ox.ac.uk For his experties in the field
	Claudio Tamagnini Universita degli Studi di Perugia claudio.tamagnini@unipg.it For his experties in the field
Opposed Reviewers:	Luigi Callisto Universita degli Studi di Roma La Sapienza Dipartimento di Ingegneria Civile Edile e Ambientale luigi.callisto@uniroma1.it He is currently working on the same topic
Additional Information:	

Question	Response
Please enter the total number of words in the article, then the number of figures and number of tables, using the following format: Total words: (Main text = , figures, tables) The main text of the paper should be as concise as possible. The word count of General Papers should not exceed 5000 words. The word count of a submission excludes the abstract, list of notation, acknowledgements, references, tables and figure captions. Discussions, Book Reviews, and Obituaries should be less than 1000 words. Whilst Geotechnique reserves the right to publish papers of any length Authors should be aware that any submission for a General Paper that is significantly over the word limit will be subjected to pre-assessment and may be returned to the Authors for editing prior to being sent for review.	Total words: 8730 Main text 6950, 19, 5
Have you included a full notation list including definitions (and SI units of measurement where appropriate) for any mathematical terms and equations included in your paper?	Yes
Upon acceptance of the article: Once the article has been accepted, we will require a completed **copyright transfer form**. You can include a completed copyright transfer form now to save from uploading it at the acceptance stage. This is required for all accepted publications and can be found here. Further information is available here.	Yes
Are your figures clear when printed in	Yes

black and white? (For example, are plot lines distinguishable; are tints sequentially graded?) As this journal is printed in black and white, any figures that are unclear may be removed.	
Are your references in Harvard style? Our reference guidelines can be found here.	Yes
To ensure your paper is indexed correctly – and therefore as discoverable as possible – in our ICE Virtual Library, please choose up to 6 keywords from our Keywords List. This can be found here. We are unable to accept keywords that do not appear on this list.	Shallow foundations, clayey soils, consolidation, macroelement modelling, bearing capacity
Have you included a caption list for all of your figures and tables?	Yes
Are your figures submitted correctly? Please note that we would prefer that your figures and tables are embedded inline in the text at first submission. We will only require that your figures are uploaded as individual, high resolution files upon acceptance. If you are submitting this article on revision, and the article has been accepted, please submit your figures separately and either in high-resolution .tiff (ideal for photographs) or .eps files (best for line drawings). Our figure requirements can be found here.	Yes
Please enter the estimated published page count for your article. This can be calculated by dividing the total number of words by 1100. Then include the total number of figures and tables divided by three.	16

Example: Article contains 5100 words, 10 figures and 3 tables (5100 words ÷ 1100) + (13 figures and tables ÷ 3) = 8.97 pages **Estimated page count is 9 pages.** Please always round up.	
Manuscript Classifications:	FOUNDATIONS AND SOIL-STRUCTURE INTERACTION
Author Comments:	

Dear Editor,

please find here attached a paper that I consider to be interesting for the Journal readers since it generalizes the macroelement approach by introducing the hydro-mechanical coupling. In the paper the authors propose a new non-dimensional generalized constitutive relationship suitable for shallow foundations on cohesive soil strata capable of predicting the evolution of settlements with time according to the imposed loading rate. All the model parameters are obtained, once and for all, by following an upscaling procedure. The parameter values can be computed once the geometry and the soil mechanical properties are assigned. For this reason, to employ the model, the designer only has to characterize the soil mechanical behaviour according to the Modified Cam Clay model and to make dimensional the model results. According to me, the proposed model may be practically employed as a design tool to assess the mechanical response of shallow foundations in both an ultimate limit state perspective and in a displacement based design framework.

Your sincerely

Claudio di Prisco

Comments and feedback received from external peer review: Assessor: Although the manuscript has improved Reviewer#2 is not entirely satisfied because some parts of the response are very general and do not address the issues raised in sufficient depth. Therefore authors are asked to further improve the manuscript and be more specific with respect to the arguments put forward by the reviewer.	
Reviewer #2: Overview of the revision: The authors have addressed most reviewers' comments and improved their manuscript, mainly clarifications (such as an introduction for section 2 to justify section 2.1) and guidance for practical employment of the method (section 4). This reviewer thinks that the authors should still clarify why they state that failure is not achieved in certain cases and the implications of using a circular cross section of the yield function in deviatoric plane for a plane strain problem. Therefore, revision of the manuscript is proposed.	
Assessor's comment about circular cross section of the yield function in deviatoric plane. This reviewer thinks that the authors' reply is very general. This reviewer suggests that the authors should clearly mention this problem and its implications in the manuscript and could mention that the M value to be used in this case should be adjusted or fitted for plane strain conditions (e.g. relationship between M value for triaxial compression and plane strain conditions).	For the sake of clarity, the following sentences were added in the text (§4): **As was previously mentioned (§2.3), the numerical results were obtained by considering a circular cross section for the Modified Cam Clay yield function. Since a plane strain problem is considered, the M value to be employed is not the one derived from experimental standard triaxial compression tests, but this has to be reduced to account for the actual shape of the soil failure envelope in the deviatoric plane (e. g. Kirkgard & Lade, 1993).** Kirkgard, M. M., & Lade, P. V. (1993). Anisotropic three-dimensional behavior of a normally consolidated clay. Canadian Geotechnical Journal, 30(5), 848-858.
Comment 1 OK. Figure 1 is useful and of high quality, but it is not so easy to understand, position of point A is stated in the text to be on t=T=0, but in the figure, its position is somehow a bit confusing.	For the sake of clarity, Figure 1 was modified.
Comment 2 For clarity, this reviewer thinks that QLu should not be referred to as "ultimate load" or using "(ii) ultimate load is not equal to 2+pi", it may be clearer to use the term "ultimate load factor", for example.	As was suggested by the reviewer, QLu was renamed ultimate load factor.
Comment 3	For the sake of clarity the following sentences were added in §2.3.2:

The authors further develop on their explanations, but they have not checked for very large vertical displacements as suggested by this reviewer. This reviewer does not understand why failure, in the sense, of reaching the CSL is not reached and I still think it is a matter of scale (i.e. considering failure as excessive settlement and not studying very large settlements). Please, check for very large vertical displacements. For discussion, it could be beneficial that the authors could plot the stress paths at certain points (not beneath the center of the footing, e.g. where horizontal strains are null) to show that the stress paths tend to the CLS. The authors state: "As is well known, in these materials a shear failure mechanism does not develop". Please, provide references and check and clarify what it is understood by failure.	**In Figure 9 the evolution of obliquity (defined as $\sqrt{(3J_2/2)}/p'$, being J_2 the second invariant of the stress deviator) with the imposed non-dimensional stress Q for different points belonging to the foundation soil domain (Points A-G of Figure 9) are reported. Moreover, in Figure 10 the contours of the obliquity corresponding to point R of Figure 7 are also illustrated. These results clearly put in evidence that critical state is got only in the proximity of the foundation edge. The subdomain at critical state is not "closed" under the foundation, meaning that the stress on the foundation can further increase (positive inclination in the Q-q curve of Figure 7). It is worth mentioning that the dimensional displacement value associated with point R is approximately 3m (while the footing width is 2m).** **For the sake of completeness, the authors also performed an additional analysis in which a larger load value (Q=60) was applied on the foundation. Even in that case, although (i) the dimension of the subdomain at critical state was larger and (ii) the foundation displacements were approximately 7m, a shear failure mechanism did not develop. In principle, a further increase in the load, to reach the critical state in sufficiently large subdomain under the foundation, could be imposed. Nevertheless, the associated displacements would be unacceptable, violating the hypothesis of small displacements. In addition, in case a large displacement approach was employed, the progressive update of the foundation position would cause a well-known (Nova and Montrasio, 1991) second order stabilizing effect.** Nova, R., & Montrasio, L. (1991). Settlements of shallow foundations on sand. Géotechnique, 41(2), 243-256.
For example, in Figure 19, it is strange that DBD uses Eq. (25) and then for ULS two options exist with Eq. (35) and again Eq. (25). Is the ULS case with Eq. (25) not really a DBD case?	Equation 35 has been derived under the assumption of constant loading rate (υ). In a general case, υ not constant (typical is the case of piecewise linearly increasing stress) even the ultimate load has to be evaluated by integrating Equation 25.
Comment 4b A design flow chart has been added (Figure 19), but not a real application example.	For the sake of completeness, an appendix (Appendix 2), containing an application example, was added.
Comment 7 The influence of the H value on the (dimensional) settlement could be clarified in the text of the manuscript.	The following sentences were added in 2.3.2: **Finally, it is worth mentioning that for very large q values, the drained mechanical response is affected by the H/B ratio value, because of the progressive downward development of the plastic zone. This dependency, has been quantitatively**

	appreciated by the authors by comparing the results (here omitted for the sake for the sake of brevity) obtained by performing additional numerical analyses in which the spatial domain was doubled along both horizontal and vertical direction, whereas B has kept constant. This dependence is negligible for displacements lower than 3B and for this reason in the constitutive relationship this effect was not taken into account.
Comment 10 Thank you for the explanation. Could a suitable reference be added in text of the manuscript?	As was suggested by the reviewer, the following reference was added: Viggiani, C. (1967). Sulle condizioni iniziali del processo di consolidazione in un mezzo elastico poroso-saturo. Rivista Italiana di Geotecnica, 3 167-181

Numerical and theoretical analyses of settlements of strip shallow foundations on normally-consolidated clays under partially drained conditions

Author 1

- Luca Flessati
- Department of Civil and Environmental Engineering, Politecnico di Milano, Milan, Italy

Author 2

- Claudio di Prisco
- Department of Civil and Environmental Engineering, Politecnico di Milano, Milan, Italy

Author 3

- Fabio Callea
- Department of Civil and Environmental Engineering, Politecnico di Milano, Milan, Italy

Corresponding author

Luca Flessati

Dipartimento di Ingegneria Civile ed Ambientale Politecnico di Milano, Piazza Leonardo da Vinci 32, 20133 Milano, Italy

luca.flessati@polimi.it

Abstract

In the geotechnical community, the macroelement approach nowadays is largely considered to be a successful theoretical tool for solving soil-structure interaction problems. This approach is based on the definition of a generalized constitutive law putting in relation a small number of suitably defined generalized stress/strain variables. The macroelement formulations proposed in the literature take into consideration either drained or undrained cases, but disregard the hydro-mechanical coupling. In this paper, the authors intend to generalize the theory by introducing a new formulation for shallow foundations overpassing this limitation and capable of accounting for the influence of loading rate on the system response. To conceive and to calibrate the model, the authors numerically analysed the case of a shallow foundation positioned on a normally consolidated clayey soil stratum whose mechanical behaviour is reproduced by means of the Modified Cam Clay model.

Finally, the approach is critically discussed in the perspective of its use as designing tool according to ultimate limit state and displacement based approaches.

Keywords

Shallow foundations, clayey soils, consolidation, macroelement modelling, bearing capacity

1. Introduction

In the last thirty years, the employment of the macroelement concept to approach soil-structure interaction problems has gained popularity in the geotechnical community, in particular in offshore (Williams et al., 1998, Martin & Houlsby, 2001, Cassidy et al., 2004, Cassidy et al., 2006, Vlahos et al. 2011, Zhang et al., 2014) and seismic applications (Grange et al., 2009, Grange et al., 2011). The basic assumptions of the macroelement approach are (i) considering a rigid footing, (ii) describing the whole soil-foundation system response by means of a very few number of generalized stress/strain variables and (iii) defining a generalized coupled (among generalized stress/strain variables) and non-linear constitutive law putting in relation the ones to the others.

In the past, many authors proposed different generalized constitutive relationships suitable for reproducing either the drained (Nova & Montrasio 1991, Montrasio & Nova, 1997, Gottardi et al., 1999, Houlsby & Cassidy, 2002, Bienen et al., 2006, Grange et al., 2008, Grange et al., 2009, Salciarini & Tamagnini, 2009, Salciarini et al., 2011, Tamagnini et al., 2011, Pisanò et al., 2016) or the undrained (Williams et al., 1998, Martin & Houslby, 2001, Cassidy et al., 2004, Cassidy et al., 2006, Grange et al., 2009, Grange et al., 2011, Vlahos et al., 2011, Zhang et al., 2014, di Prisco & Flessati, 2020) foundation response. In practice, all these authors assumed the loading rate to be, with respect to the system consolidation rate, either very low (drained case) or very high (undrained case).

In this paper, the authors propose a new non-dimensional generalized constitutive relationship conceived in the framework of the macroelement theory capable of taking into account the hydro-mechanical coupling and the influence of the loading rate on the mechanical response of the foundation. In particular, the authors consider the case of a rigid strip shallow foundation under vertical centred loads resting on a horizontal homogeneous normally-consolidated clay stratum.

The model has been conceived by critically interpreting a large series of FEM numerical analyses results. With respect to what done in the literature (e.g. Nova & Montrasio 1991, Gottardi et al., 1999), the authors propose a different strategy to make non-dimensional the generalized kinematic and static variables (§2.2), similar these latter to that proposed in di Prisco et al. (2018) and in di Prisco et al. (2020) with reference to the mechanical response of both tunnel fronts and cavities. In detail: in §2.3 a non-dimensional time variable is suitably defined to generalize the mechanical response of the foundation under "partially drained conditions", whereas in §3 a 1D elastic-visco plastic strain hardening constitutive relationship is proposed and calibrated on the numerical results illustrated in §2. In §3 the constitutive relationship is also validated by employing the results of a series of additional numerical analyses and in §4 an engineering application of the model is suggested.

2. Numerical analyses results

As is well known, the mechanical response of shallow foundations on saturated soil strata depends not only on the final value of the applied load, but also on the loading rate, that is, generally, on the loading time history (Figure 1a).

For the sake of simplicity, in this paper (i) the strip foundation is assumed to be rigid, (ii) the applied load to be vertical and centred, (iii) only monotonic load histories are discussed and (iv) the foundation "configurational features" (Pisanò et al., 2016), such as the value of the lateral surcharge, footing embedment and underground phreatic level, do not change with time. Under these assumptions, the foundation response may be described in the σ_{sf}-u_{sf}-t space (Figure 1a), being σ_{sf}, u_{sf} and t the average stress applied on the foundation, the average foundation settlement and time, respectively.

As it was previously mentioned, the final goal of this paper is the introduction of a generalized constitutive relationship for reproducing the partially drained mechanical response of shallow strip foundations. The model will be defined by employing the non-dimensional variables Q–q–T (Figure 1b), corresponding to σ_{sf}, u_{sf} and t, respectively.

The procedure to define these non-dimensional variables is detailed here below: their definition, depending on both geometry and mechanical/hydraulic soil properties, is given for undrained conditions in §2.2 and for partially drained conditions in §2.3.

The numerical results illustrated in §2.2 are obtained by performing a series of numerical tests following stress paths (OA of Figures 1a and 1b) belonging to the t=T=0 planes and (ii) by employing in the numerical code an elastic-perfectly plastic (Tresca type) constitutive model. In contrast, all the numerical results in §2.3 are obtained (i) by imposing constant rate loads (OB of Figures 1a and 1b) and (ii) by employing a strain hardening elastic plastic constitutive relationship (Modified Cam Clay model). Finally, OBC stress paths (Figure 1) are discussed in §3.1 and §3.3. In Figure 1, for the sake of clarity, the projections of the stress paths on the three planes (t=T=0, u_{sf}=q=0 and σ_{sf} =Q=0) are also plotted.

The comparison among the numerical results illustrated in §2.2 and in §2.3 allows to the reader to appreciate the role played by the constitutive relationship in governing the definition of the non-dimensional variables: a key point of the upscaling procedure employed in this paper. This mimics what is nowadays commonly done to pass from the "microstructural" to the "macrostructural" parameters used to define constitutive relationships at the macroscale.

2.1 Numerical model

The mechanical response of a *B* wide strip foundation resting on a homogeneous saturated normally consolidated clay stratum of thickness *H* (Figure 1) is investigated by means of the commercial code Midas GTS NX. Here in the following, thickness *H*, is assumed not to affect the bearing capacity of the foundation, i.e. the lower boundary to be sufficiently far away from the ground level.

As it was previously mentioned, the soil mechanical behaviour is simulated by means of a strain hardening elastic plastic (Modified Cam Clay model) constitutive relationship, when the hydro-mechanical coupling is accounted for (§2.3), whereas when the biphasic nature of the soil is disregarded and undrained conditions are taken into consideration (§2.2), the material mechanical behaviour is instead simulated by using an elastic-perfectly plastic constitutive relationship.

The (weightless) foundation is assumed to be elastic (the Young modulus and the Poisson's ratio, representative for a concrete foundation, are imposed to be equal to 30GPa and 0.3, respectively) and the foundation-soil interface is assumed to be perfectly rough.

The soil domain is subdivided into 3400 triangular elements (Figure 2). In all the cases, quadratic shape functions are employed for the displacements, whereas for pore water pressure, in case of coupled numerical analyses, linear shape functions are employed. The dimension of the elements is not constant in the soil domain: the element size is smaller in the proximity of the foundation (Figure 2). To assess the reliability of numerical results, the influence on the results of both the domain horizontal dimension and the spatial discretization was analysed. The numerical results, demonstrating that the domain dimensions and the spatial discretization are acceptable, are hereafter omitted for the sake of brevity.

On the domain vertical boundaries, the horizontal displacements and at the domain base both vertical and horizontal displacements are not allowed. On the domain upper boundary, a uniform normal stress distribution (σ_{sf0}), reproducing the foundation embedment, is applied. In coupled numerical analyses the water table is assumed to be coincident with the foundation plane.

The numerical analyses, whose results are reported in §2.2, have been performed as it follows:

1) the initial state of stress is imposed: total vertical stresses are linearly and progressively increased to their final target value, depending this latter on both the saturated soil unit weight (γ_{sat}) and the σ_{sf0} value, whereas horizontal total stresses are progressively increased by imposing the ratio between total horizontal and total vertical stress ($\bar{k}$) to be constant. During this phase the vertical stress distribution acting on the foundation (σ_{sf}) is imposed to be coincident with σ_{sf0}.
2) σ_{sf} is progressively increased.

On the contrary, the analyses, whose results are reported in §2.3, have been performed as it follows:

1) a hydrostatic pore water pressure distribution is initially imposed;

2) the initial vertical effective state of stress is obtained by progressively increasing both gravity and σ_{sf0}, whereas the initial horizontal effective state of stress by integrating the constitutive relationship. As a consequence, the at rest lateral earth pressure coefficient (k_0) is a function of the Modified Cam Clay constitutive parameters employed (Roscoe & Burland, 1968). As in the previous case, during this phase σ_{sf} is imposed to be equal to σ_{sf0}.

3) σ_{sf} is progressively increased with time at a constant rate, hereafter named υ.

2.2 Undrained total stress numerical analyses results

In this section, the soil mechanical behaviour is reproduced by means of an elastic-perfectly plastic constitutive relationship. The failure condition is described by means of Tresca criterion (the undrained strength is hereafter named S_u) and the flow rule is assumed to be associated. For the sake of simplicity, both S_u and the elastic soil properties (undrained Young modulus E_u and undrained Poisson's ratio ν_u=0.495) are assumed to be constant along depth.

To analyse the mechanical response of the system, different geometries and soil mechanical properties were considered (Table 1). The reference case is UD_1. In all the other cases only one parameter has been changed (bolded in Table 1).

It is worth mentioning that σ_{sf0}, related the foundation embedment, may be interpreted as a sort of geometrical parameter. All the cases summarized in Table 1 are associated with $\bar{k}$=1.

	B (m)	σ_{sf0} (kPa)	E_u (MPa)	S_u (kPa)
UD_1	2	20	5	20
UD_2	2	20	5	**10**
UD_3	2	20	**2**	20
UD_4	**4**	20	5	20
UD_5	2	**40**	5	20

Tab 1: Geometrical/mechanical parameters (UD_1 is the reference case, the parameter bolded values represent the ones changed with respect to the reference case)

Analogously to what presented in di Prisco et al. (2018, 2020) for deep tunnel cavities and fronts, the foundation response is illustrated by employing a non-dimensional "characteristic curve" putting in relation the following variables:

$$Q = \frac{\sigma_{sf} - \sigma_{sf0}}{S_u}, \qquad \text{1a.}$$

$$q = \frac{u_{sf}}{u_{sf,el}} \frac{q_{lim} - \sigma_{sf0}}{S_u}, \qquad \text{1b.}$$

being u_{sf} the average foundation displacement, q_{lim} the bearing capacity, whereas $u_{sf,el}$ is the elastic displacement corresponding to σ_{sf}=q_{lim}. To calculate $u_{sf,el}$ the following expression was employed:

$$u_{sf,el} = \frac{q_{lim} - \sigma_{sf0}}{E_u} B I_w, \qquad \text{2.}$$

where the non-dimensional parameter I_w (Giroud, 1972) takes into account the *H/B* ratio value. The value of I_w corresponding to H/B=5 is 1.02, whereas for $H/B \rightarrow 0$, I_w goes to zero.

The numerical characteristic curves (corresponding to UD_i, i=1,5) of Figure 3a clearly show that the system response plotted in the non-dimensional *Q*-*q* plane is not affected by (i) geometry, (ii) soil mechanical properties and (iii) σ_{sf0}. It is also evident that the initial response is linear and elastic (the initial slope is equal to 1) and **the non-dimensional limit load (ultimate load factor) equal to 2+π**. This result, coincident with the one obtained by employing the limit analysis theory, puts in evidence that the influence of (elastic) strains on the ultimate load factor is negligible.

For the sake of completeness, in Figure 3b the influence of $\bar{k}$ is discussed (case UD_1 of Table 1). As was expected, the initial elastic response and the ultimate load factor are not affected by $\bar{k}$. $\bar{k}$ only influences the value of Q for which the transition from the linear and to the non-linear response occurs (di Prisco et al., 2018).

2.3 Partially drained numerical analyses results

In this section, the soil mechanical behaviour is reproduced by means of the Modified Cam Clay model. Both the yield function and the plastic potential are characterized in the deviatoric plane by a circular cross section. As far as the elastic behaviour is concerned, a pressure dependent elastic bulk modulus and a constant Poisson's ratio (ν) value are assumed. The model constitutive parameters are thus λ (virgin loading line inclination), κ (unloading-reloading line inclination), M (critical state line slope), e_0 (initial void ratio) and ν. Permeability k is assumed to be constant within the soil stratum.

A series of numerical analyses by considering different geometries, mechanical and hydraulic parameters, soil submerged unit weight (γ') and loading rate values (Table 2) was performed. The reference case is PD_1; in all the other cases, the parameters in Table 2 with values not coincident with those employed in PD_1 are bolded.

	B (m)	σ_{sf0} (kPa)	M (-)	κ (-)	κ/λ (-)	k (m/s)	γ' (kN/m^3)	υ (kPa/ day)	t_l (day)	Final σ_{sf} value (kPa)	T_l (-)
PD_1	2	20	1	0.05	0.2	10^{-8}	10	6	7.7	46	0.16
PD_2	2	20	1	0.05	0.2	**$2\cdot10^{-8}$**	10	***12***	3.8	46	0.16
PD_3	2	20	1	0.025	0.2	**$0.5\cdot10^{-8}$**	10	***6***	7.6	46	0.16
PD_4	2	20	1	***0.025***	0.2	10^{-8}	10	***12***	3.8	46	0.16
PD_5	2	20	1	0.05	0.2	10^{-8}	10	**60**	0.65	39	0.012
PD_6	2	20	1	0.05	0.2	10^{-8}	10	***6000***	0.065	39	$1.2\cdot10^{-4}$
PD_7	2	20	1	**0.025**	0.2	10^{-8}	10	*60*	0.65	39	0.024
PD_8	2	20	1	0.05	***0.1***	10^{-8}	10	60	0.62	37	0.011
PD_9	2	20	1	0.05	***0.4***	10^{-8}	10	60	0.73	44	0.014
PD_{10}	2	20	***0.8***	0.05	0.2	10^{-8}	10	60	0.53	32	0.01
PD_{11}	2	20	***1.2***	0.05	0.2	10^{-8}	10	60	0.75	45	0.014
PD_{12}	2	***10***	1	0.05	0.2	10^{-8}	10	60	0.38	23	0.007
PD_{13}	2	***40***	1	0.05	0.2	10^{-8}	10	60	1.18	71	0.022
PD_{14}	***3***	20	1	0.05	0.2	10^{-8}	10	60	0.71	43	0.006
PD_{15}	***4***	20	1	0.05	0.2	10^{-8}	10	60	0.77	46	0.004
PD_{16}	2	20	1	0.05	0.2	10^{-8}	***8***	60	0.63	38	0.012
PD_{17}	2	20	1	0.05	0.2	10^{-8}	***12***	60	0.68	41	0.013
PD_{18}	2	20	1	0.05	0.2	10^{-8}	10	***2.4***	22.5	54	0.42
PD_{19}	2	20	1	0.05	0.2	10^{-8}	10	***0.8***	138	110	2.55
PD_{20}	2	20	1	0.05	0.2	10^{-8}	10	***0.4***	475	190	8.8
PD_{21}	2	20	1	0.05	0.2	10^{-8}	10	***0.2***	1115	223	20.7
PD_{22}	2	20	1	0.05	0.2	10^{-8}	10	***0.006***	40000	240	745
PD_{23}	2	20	1	0.05	0.2	10^{-8}	10	***0.001***	240000	240	4460

Tab 2: Geometrical/mechanical/hydraulic parameters, soil unit weight and loading rate values (e_0=0.5, ν=0.3). PD_1 is the reference case, the parameter values in italics represent the ones changed with respect to the reference case

Analogously to what proposed in Flessati & di Prisco (2018) and in di Prisco et al. (2019) for tunnel fronts excavated under partially drained conditions, the partially drained foundation response is interpreted by employing the non-dimensional variables introduced in the undrained case (Equations 1a and 1b). In this case, when a strain hardening elastic plastic constitutive relationship is used, the undrained strength is not a material property but depends on both the initial (geostatic) effective pressure and the imposed loading path. Since in the boundary value problem here considered, (i) the initial effective pressure varies with depth and (ii) since different points belonging to the spatial domain follow different loading paths, each material point is associated with a different S_u value. Nevertheless, for the sake of simplicity, to define the non-dimensional variables Q and q, the authors decided to consider the S_u value analytically calculated by integrating the Modified Cam Clay constitutive equations under standard undrained triaxial compression stress paths:

$$S_u = \frac{M}{2^{2-\kappa/\lambda}} p_0' = \frac{M}{2^{2-\frac{\kappa}{\lambda}}} \frac{1+2k_0}{3} \left(\frac{\gamma' B}{2} + \sigma_{sf0} \right) \qquad 3.$$

and by evaluating p_0' as the (oedometric) value of the effective pressure at a depth equal to $B/2$, whereas the at rest lateral earth pressure coefficient k_0 was numerically estimated from the stress initialization step. It is worth mentioning that a very satisfactory agreement between the numerical values of k_0 and the values estimated by employing the analytical expression proposed by Roscoe & Burland (1968) was retrieved.

In contrast with what assumed in §2.2, also the elastic properties vary with the effective pressure. $u_{sf,el}$ (Equation 1b) is therefore arbitrarily calculated by using Equation 2 in which E_u is evaluated at a depth equal to $B/2$ from Cam Clay elastic constitutive parameters κ as it follows:

$$E_u = \frac{9}{2} \frac{1+e_0}{\kappa} \frac{1-2\nu}{1+\nu} p_0' = \frac{9}{2} \frac{1+e_0}{\kappa} \frac{1-2\nu}{1+\nu} \frac{1+2k_0}{3} \left(\frac{\gamma' B}{2} + \sigma_{sf0} \right) \qquad 4.$$

To discuss the influence of loading time on the foundation response, the non-dimensional time:

$$T = \frac{c_{v2} t}{B^2} \qquad 5.$$

has been introduced, being t the physical time and

$$c_{v2} = \frac{kE}{2\gamma_w(1+\nu)(1-2\nu)}, \qquad 6.$$

the consolidation coefficient under 2D conditions (Viggiani, 1967), γ_w the water unit weight and E the elastic Young modulus calculated at a depth of $B/2$:

$$E = 3\frac{1+e_0}{\kappa}(1-2\nu)p'_0 = 3\frac{1+e_0}{\kappa}(1-2\nu)\frac{1+2k_0}{3}\left(\frac{\gamma' B}{2} + \sigma_{sf0}\right) \qquad \mathbf{7.}$$

The four superimposed curves of Figure 4 are obtained by considering different c_{v2}, loading time ($t_l = \bar{\sigma}_{sf}/v$, being $\bar{\sigma}_{sf}$ the final value of σ_{sf}) but keeping constant:

(i) the non-dimensional loading time (Figure 1b):

$$T_l = \frac{c_{v2} t_l}{B^2}, \qquad 8.$$

(ii) and all the remaining constitutive parameters.

In Equation 5 c_{v2} is assumed to be a function of the elastic volumetric compliance, that is the plastic volumetric contribution is neglected. As is observed in Flessati & di Prisco (2018), this hypothesis is acceptable since volumetric plastic strain increments at critical state are nil and in most of the plastified spatial subdomain the material is at the critical state. This implies that the role of plasticity in the hydro-mechanical coupling is in average almost negligible.

2.3.1 Undrained response

The numerical results obtained for sufficiently low values (to ensure an ideal undrained response) of T_l ($T_l \leq 0.024$) and different κ, κ/λ, M, σ_{sf0}, B and γ' values (PD_5-PD_{17} of Table 2) are summarized in Figure 5. The results illustrated in Figure 5 emphasise the role of both geometry and material mechanical properties in affecting the system response under undrained condition, that is for $T_l \to 0$.

As is evident (Figure 5a), for $T_l < 0.024$ (PD_5-PD_7) all the curves are superimposed: the response is practically undrained and, in the *Q*-*q* plane, the system response is not influenced by the elastic soil property values.

In contrast, the results illustrated in Figures 5b-5f allow to conclude that (i) mechanical property values, geometry and soil unit weight mainly affect the ultimate load factor value (Q_{Lu}) and (ii) the ultimate load factor is not equal to 2+π. By representing the dependency of Q_{Lu} on σ_{sf0}, γ' and *B* (the corresponding graphs are here omitted for the sake of brevity), it is possible to derive that Q_{Lu} is a linear function of all these quantities. This is due to the fact that, in contrast with what assumed in §2.2, for a normally consolidated material, according to the Modified Cam Clay model, the soil strength linearly depends on the initial effective pressure. Q_{Lu} has been observed to depend on *B*, σ_{sf0} and γ' even by Davis & Booker (1973), who analysed foundations placed on strata with linearly increasing undrained strength with depth.

For these reasons, the authors have decided to calculate Q_{Lu} as it follows:

$$Q_{Lu} = \frac{q_{lim} - \sigma_{sf0}}{s_u} = \frac{\sigma_{sf0} N_q^* + \frac{1}{2} B \gamma' N_\gamma^* - \sigma_{sf0}}{s_u} = \frac{\sigma_{sf0}(N_q^* - 1) + \frac{1}{2} B \gamma' N_\gamma^*}{s_u} \qquad 9.$$

where N_q^* and N_γ^* are new undrained Cam Clay bearing capacity coefficients, depending on Cam Clay constitutive parameters. The numerical FEM results performed by the authors allow to define the dependence of these coefficients on *M* and κ/λ (Figures 6a and 6b).

To validate Equation 9, in Figure 6c the Q_{Lu} numerically calculated ($Q_{Lu,FEM}$) are compared with those obtained by employing Equation 9 ($Q_{Lu,th}$). As is evident, the agreement is very satisfactory.

2.3.2 Partially drained response

In this subsection, the FEM numerical results obtained by performing OB loading paths (Figure 1b), are illustrated. The dependence of Q-q curves on T_l is illustrated in Figure 7. The constitutive parameters employed are those of Table 2. To better appreciate the initial part of the characteristic curves, in Figure 7b a magnification of Figure 7a is reported.

As was previously mentioned, the curves corresponding to cases PD_5 and PD_6 are superimposed and refer to the undrained system response. In contrast, the curves corresponding to cases PD_{22} and PD_{23} (T_l=745 and 4460, respectively), corresponding to the drained case, are also superimposed. For the other cases ($0.16< T_l <20.7$) the system response is significantly affected by the loading rate. In particular, all the curves for T_l<0.42 are characterized by a horizontal asymptote, corresponding to the development of a shear failure mechanism, whereas all the others are characterized by a continuous hardening since in the soil domain a failure mechanism does not develop and the plastic domain spatially downward propagates, according to a punching mechanism.

The difference in shape of the characteristic curves is due to different strain and displacement fields developing in the soil spatial domain. For the sake of brevity, in Figures 8 and 9 strain fields and vertical displacements on the ground surface (displacements are normalized by employing Equation 1b) are plotted only in case of PD_6 (Table 2) and PD_{23} (Table 2). In particular, Figures 8a, 8c, 8e and 9a correspond to point P (of PD_6), whereas Figures 8b, 8d, 8f and 9b to point R (of PD_{23}), respectively.

As is evident, in Figures 8a, 8c and 8e, for large loading rates, strains mainly accumulate in the foundation proximity and in shallower zones of the soil domain. A plastic shear failure mechanism develops (Figure 8a), reaching a stationary spatial configuration. In contrast, when the loading rate value is sufficiently small (Figures 8b, 8d and 8f), a punching mechanism seems to take place and plastic strains are diffused in a large plastic deep zone under the foundation (Figure 8b), continuously expanding in space.

In Figure 9 the evolution of obliquity (defined as $\sqrt{3J_2/2}/p'$, being J_2 the second invariant of the stress deviator) with the imposed non-dimensional stress Q for different points belonging to the foundation soil domain (Points A-G of Figure 9) are reported. Moreover, in Figure 10 the contours of the obliquity corresponding to point R of Figure 7 are also illustrated. These results clearly put in evidence that critical state is got only in the proximity of the foundation edge. The subdomain at critical state is not "closed" under the foundation, meaning that the stress on the foundation can further increase (positive inclination in the Q-q curve of Figure 7). It is worth mentioning that the dimensional displacement value associated with point R is approximately 3m (while the footing width is 2m).

For the sake of completeness, the authors also performed an additional analysis in which a larger load value (Q=60) was applied on the foundation. Even in that case, although (i) the dimension of the subdomain at critical state was larger and (ii) the foundation displacements were approximately 7m, a shear failure mechanism did not develop. In principle, a further increase in the load, to reach the critical state in sufficiently large subdomain under the foundation, could be imposed. Nevertheless, the associated displacements would be unacceptable, violating the hypothesis of small displacements. In addition, in case a large displacement approach was employed, the progressive update of the foundation position would cause a well-known (Nova and Montrasio, 1991) second order stabilizing effect.

According to the authors, the comparison of the numerical results allows to state that the shear failure mechanism developing for small T_l values, is inhibited in case of large T_l values by the development of vertical strains in the deeper layers of the soil stratum, due to the strain hardening constitutive relationship adopted to model the soil behaviour: under drained conditions, the pre-failure mechanical behaviour of the soil (the material deformability) does not allow the development of a standard global (shear) failure mechanism (Figure 8b relative to point R of test PD_{23}). In contrast, if an elastic-perfectly plastic Mohr-Coulomb constitutive relationship was employed, even under drained conditions, a failure mechanism and a limit value for the bearing capacity would be obtained. The authors have performed these analyses also by using a Mohr Coulomb elastic-perfectly plastic constitutive relationship, but, for the sake of brevity, these numerical results are here omitted.

A further confirmation of what observed here above is given in Figure 10 where the vertical displacement profiles referred to undrained (Figure 10a) and drained (Figure 10b) tests are compared. In Figure 10a the lateral upward vertical displacements testify the mechanism development, whereas in Figure 10b the downward displacements testify the effect of the progressive compaction of deep layers due to the lateral propagation in the deeper zones of the plastified zone.

Finally, it is worth mentioning that for very large q values, the drained mechanical response is affected by the H/B ratio value, because of the progressive downward development of the plastic zone. This dependency, has been quantitatively appreciated by the authors by comparing the results (here omitted for the sake for the sake of brevity) obtained by performing additional numerical analyses in which the spatial domain was doubled along both horizontal and vertical direction, whereas B has kept constant. This dependence is negligible for displacements lower than 3B and, for this reason, in the constitutive relationship presented in the following section this effect was not taken into account.

3. Definition of the generalized non-dimensional constitutive law

In this section, a constitutive relationship conceived in the framework of the macroelement theory to reproduce the partially drained foundation response is proposed. The model is defined in terms of Q, q and T (Equations 1a, 1b and 5, respectively), that is in the non-dimensional space of Figure 1b.

The main assumption of the constitutive relationship consists in assuming an in series scheme (Figure 11), where submodel 1 refers to perfectly undrained, whereas submodel 2 to perfectly drained conditions, respectively.

As is schematized in Figure 11:

$$dq = dq_u + dq_d, \qquad 10.$$

where q_u and q_d are the non-dimensional displacements associated with undrained and drained conditions, respectively, whereas symbol *d* stands for increment.

Both dq_u and dq_d are obtained by adding a reversible/elastic (dq_u^{el} and dq_d^{el}) to an irreversible/plastic (dq_u^{pl} and dq_d^{pl}) contribution. To take the progressive dissipation of the in excess pore water pressure into account, a viscous damper (submodel 3), in parallel with the elastic spring and the plastic slider describing the drained response, is introduced (Figure 11). In the in parallel system, the non-dimensional stress increment dQ is subdivided into the sum of two terms:

$$dQ = dQ' + dU \qquad 11.$$

where dQ is the non-dimensional stress increment, dQ' and dU the non-dimensional generalized stress increments acting on the drained element (submodel 2) and on the viscous damper, respectively (Figure 11).

As far as undrained submodel 1 (Figure 11) is concerned,

$$dq_u^{el} = \frac{1}{K_u^{el}} dQ, \qquad 12.$$

being K_u^{el} the elastic undrained stiffness, whereas the plastic slider response is obtained once yield function (f_u) and plastic potential (g_u) are defined. In particular:

$$f_u = g_u = Q - Q_u = 0, \qquad 13.$$

where Q_u is the hardening variable, depending on plastic strain increments as it follows:

$$dQ_u = \alpha_u \left(1 - \frac{Q_u}{Q_L}\right) dq_u^{pl} + dQ_d, \qquad 14.$$

being α_u a non-dimensional constitutive parameter, Q_d the drained hardening variable (Equations 19 and 20) whereas Q_L is an internal variable, whose evolution is given here below.

Equation 14 is an extension of Butterfield law (Butterfield, 1980), where:

(i) the limit load value (Q_L) is linearly evolving with drained plastic strains q_u^{pl} (Equation 19):

$$Q_L = Q_{Lu} + \beta_d q_d^{pl}, \qquad 15.$$

being Q_{Lu} and β_d two non-dimensional constitutive parameters. This implies that the progressive accumulation of irreversible drained strains may inhibit the development of the current undrained failure mechanism (hydro-mechanical coupling), that is the material consolidation causes an increase in the undrained material strength.

(ii) The hardening of Q_u (Equation 11) is inhibited by the accumulation of drained strains, that is the evolution of Q_d. In fact, by employing both the standard flow rule and the consistency condition, from Equation 14 it follows:

$$dq_u^{pl} = \frac{1}{\alpha_u} \frac{Q_L}{Q_L - Q} \langle dQ - dQ_d \rangle. \qquad 16.$$

This implies that no undrained plastic generalized strains develop when $dQ=dQ_d$, that is when the load is applied very slowly and excess pore water pressure does not accumulate within the system (dU=0).

By summarizing, the undrained constitutive law (element 1 of Figure 11) can be thus written as follows:

$$dq_u = dq_u^{el} + dq_u^{pl} = \frac{1}{K_u^{el}} dQ + \frac{1}{\alpha_u} \frac{Q_L}{Q_L - Q} \langle dQ - dQ_d \rangle. \qquad 17.$$

As far as the drained response is concerned (submodel 2 of Figure 11), the elastic response is given by:

$$dq_d^{el} = \frac{1}{K_d^{el}} dQ', \qquad 18.$$

being K_d^{el} the elastic drained stiffness, whereas the plastic slider constitutive relationship is obtained again once yield function (f_d), plastic potential (g_d) and hardening rule are assigned:

$$f_d = g_d = Q' - Q_d = 0, \qquad 19.$$

$$dQ_d = \left[\frac{\exp\left(\frac{Q_d}{\alpha_d}\right)}{K_d^{ep}} - \frac{1}{K_d^{el}} \right]^{-1} dq_d^{pl}, \qquad 20.$$

being K_d^{ep} and α_d two non-dimensional constitutive parameters. The hardening rule, never nullifying, is inspired to that employed by the authors to describe the characteristic curves for deep tunnel cavities and fronts (Carter et al, 1986, di Prisco et al., 2018 and di Prisco & Flessati, 2020) and is intended to reproduce the structural hardening associated with the continuous spatial expansion of the plastic zone within the deeper zone of the underneath soil (punching mechanism).

By imposing flow rule and consistency condition:

$$dq_d^{pl} = \frac{\exp\left(\frac{Q_d}{\alpha_d}\right)}{K_d^{ep}} dQ' - \frac{1}{K_d^{el}} dQ' \qquad 21.$$

And therefore:

$$dq_d = dq_d^{el} + dq_d^{pl} = \frac{\exp\left(\frac{Q_d}{\alpha_d}\right)}{K_d^{ep}} dQ' = \frac{\exp\left(\frac{Q_d}{\alpha_d}\right)}{K_d^{ep}} (dQ - dU) \qquad 22.$$

Finally, as far as the viscous damper is concerned (sub model 3 of Figure 11), the following expression is adopted:

$$U = \eta \frac{dq_d}{dT}, \qquad 23.$$

being η is a non-dimensional constitutive parameter. It is worth mentioning that, since the constitutive law is written by employing non-dimensional quantities (Q, q and T), the constitutive parameter η does not depend on (i) soil mechanical and (ii) hydraulic properties and (iii) geometry.

For the proposed constitutive model, U may be interpreted as an internal variable: its evolution may be in fact obtained by combining Equations 11, 22 and 23:

$$\frac{dU}{dT} = \frac{dQ}{dT} - C(Q,U) = \frac{dQ}{dT} - \frac{U}{\eta} \frac{K_d^{ep}}{\exp\left(\frac{Q-U}{\alpha_d}\right)} \qquad 24.$$

As is evident, dU is given by the sum of two terms. The first one (dQ) is a source term, associated with the application of the load on the strip footing, whereas the second one (CdT) is a dissipation term, associated with the spatial diffusion and the water drainage. For very large values of dQ/dT, $dU/dT \approx dQ/dT$, implying $dQ'/dT = 0$.

By combining Equations 17, 22 and 24 the global constitutive relationship becomes:

$$dq = \boldsymbol{A}^T \boldsymbol{X}, \qquad 25.$$

being

$$\boldsymbol{X} = \begin{bmatrix} dQ \\ dT \end{bmatrix}, \qquad 26a.$$

$$\boldsymbol{A} = \begin{bmatrix} A_1(Q,U) \\ A_2(Q,U) \end{bmatrix}, \qquad 26b.$$

where

$$A_1(Q,U) = \begin{cases} \frac{1}{K_u^{el}} + \frac{1}{\alpha_u} \frac{Q_{Lu+\beta_d}\left[\frac{\alpha_d}{K_d^{ep}}\exp\left(\frac{Q-U}{\alpha_d}\right)-\frac{Q-U}{K_d^{el}}\right]}{Q_{Lu+\beta_d}\left[\frac{\alpha_d}{K_d^{ep}}\exp\left(\frac{Q-U}{\alpha_d}\right)-\frac{Q-U}{K_d^{el}}\right]-Q} & dQ > dQ' \\ \frac{1}{K_u^{el}} & dQ < dQ' \end{cases}, \qquad 27a.$$

$$A_2(Q,U) = \begin{cases} \frac{U}{\eta} - \frac{U}{\eta} \frac{K_d^{ep}}{\exp\left(\frac{Q-U}{\alpha_d}\right)} \frac{1}{\alpha_u} \frac{Q_{Lu+\beta_d}\left[\frac{\alpha_d}{K_d^{ep}}\exp\left(\frac{Q-U}{\alpha_d}\right)-\frac{Q-U}{K_d^{el}}\right]}{Q_{Lu+\beta_d}\left[\frac{\alpha_d}{K_d^{ep}}\exp\left(\frac{Q-U}{\alpha_d}\right)-\frac{Q-U}{K_d^{el}}\right]-Q} & dQ > dQ' \\ \frac{U}{\eta} & dQ < dQ' \end{cases} \qquad 27b.$$

The analytical passages to obtain Equation 25 are detailed in Appendix 1.

Equation 25 may be integrated by using an explicit integration scheme. All the results reported in the following section were obtained by subdividing the loading process into 10000 steps (the solutions obtained for larger numbers of steps are practically identical) and the computational time, because of the simplicity of the algorithm, is totally negligible.

In Equations 25-27, dQ is implicitly assumed to be the controlled variable, whereas dq and dU to be the response variables. In case of an ideal displacement controlled test, Equations 24 and 25 can be rewritten as follows:

$$dU = \frac{dq}{A_1(Q,U)} - \left[\frac{A_2(Q,U)}{A_1(Q,U)} + C(Q,U)\right] dT, \qquad 28a.$$

$$dQ = \frac{dq}{A_1(Q,U)} - \frac{A_2(Q,U)}{A_1(Q,U)} dT, \qquad 28b.$$

3.1 Constitutive parameters

The generalized constitutive relationship is characterized by 8 “macro” constitutive parameters: 3 (K_u^{el}, α_u, Q_{Lu}) define the undrained response, 3 (K_d^{el}, K_d^{ep} and α_d) the drained one, one (η) defines the damper response and the last one (β_d) the evolution of internal variable Q_L. In addition, the initial values for Q_u and Q_d (Q_{u0} and Q_{d0}, respectively) have to be assigned to integrate the constitutive relationship. In this paper, a shallow foundation resting on a normally consolidated clayey soil stratum is considered. In this case, irreversible strains develop from the very beginning of the loading process, thus both Q_{u0} and Q_{d0} are imposed to be nil.

Among the 8 macro constitutive parameters, 7 (Table 3) are assumed not to depend on geometry and mechanical properties. Their values have been determined on the numerical results once and for all. This is possible owing to the non-dimensional variables definitions (Equations 1a, 1b and 5) employed.

On the contrary, Q_{Lu} depends on *B*, σ_{sf0}, soil mechanical properties (*M*, λ/κ) and soil unit weight (γ'). Nevertheless, as was already mentioned (§2.3), its value may be calculated by means of Equation 9.

Here below, the procedure to assign the values, the 7 constitutive parameters listed in Table 3 is briefly outlined.

K_u^{el}	α_u	K_d^{el}	K_d^{ep}	α_d	η	β_d
1.1	1.35	1.18	0.13	90	0.095	*0.123*

Tab. 3: Macro constitutive parameters

In case of undrained conditions ($T_l \to 0$), $dQ = dU$ and $dQ' = 0$. In this case, the system response can be schematized with the rheological model of Figure 12a and, from Equations 10, 16 and 22:

$$dq = \left(\frac{1}{K_u^{el}} + \frac{1}{\alpha_u}\frac{Q_{Lu}}{Q_{Lu}-Q}\right)dQ. \qquad 29.$$

Equation 29 only depends on three constitutive parameters: K_u^{el}, Q_{Lu} and α_u.

K_u^{el} is calibrated by using the numerical results of an elastic analysis in which the elastic bulk modulus increases with confining pressure. The parameters employed are not important since K_u^{el} does not depend on them. Once K_u^{el} is calculated, the α_u value may be calculated from the initial slope of the undrained characteristic curve in the *Q*-*q* plane.

In fact, for Q=0 Equation 29 may be written as:

$$\frac{dQ}{dq} = \frac{K_u^{el}\alpha_u}{K_u^{el}+\alpha_u} \qquad 30.$$

The comparison between the undrained FEM numerical results (case PD_6 of Table 2) and Equation 25, in which K_u^{el}=1.1 and α_u=1.35 (Table 3) are employed, is reported in Figure 12b.

In case of drained conditions, ($T_l \rightarrow +\infty$), $dQ = dQ'$ and $dU = 0$. In this case, from Equation 17 $dq_u^{pl} = 0$. Therefore (Figure 13a), according to Equations 10, 17 and 22:

$$dq = \left[\frac{1}{K_u^{el}} + \frac{\exp\left(\frac{Q}{\alpha_d}\right)}{K_d^{ep}}\right] \mathrm{dQ}. \qquad 31.$$

Equation 31 depends on three parameters: K_u^{el} (already determined), K_d^{ep} and α_d. For $Q = 0$, Equation 31 reduces to

$$dq = \left[\frac{1}{K_u^{el}} + \frac{1}{K_d^{ep}}\right] \mathrm{dQ}. \qquad 32.$$

This implies that parameter K_d^{ep} can be calculated from the initial slope in the *Q*-*q* plane of the drained characteristic curve. Once $K_d^{ep}$is evaluated, for large Q values α_d is assessed.

The comparison between drained numerical FEM results (case PD_{23} of Table 2) and the constitutive relationship prediction (solid line), in which $K_d^{ep} = 0.13$ and α_d=90 (Table 3) are employed, is reported in Figure 13b.

Analogously to what done for K_u^{el}, K_d^{el} has been numerically evaluated by employing the results of an ad hoc elastic FEM numerical analyses (Table 3). In this case, K_d^{el} depends on the drained ν value. Since ν is assumed not to significantly vary for natural soils, here in the following K_d^{el}will be assumed not to depend on soil properties.

The value of parameter β_d is obtained (i) by employing Equation 15, (ii) by neglecting elastic accumulated drained displacements:

$$Q_L \approx Q_{Lu} + \beta_d q_d, \qquad 33.$$

and (iii) by performing a series of FEM numerical analyses suitably designed to describe the dependency of Q_L on q_d (Equation 33). It is about of a series of stepwise load controlled tests (multi stage test Figure 14a, analogous to the experimental and numerical tests reported in Zdravković et al., 2003, Gourvenec et. al, 2014 and Fu et al. 2015), where undrained loading phases (OA paths of Figure 1b) were followed by consolidation phases during which the value of the applied load is kept constant (BC paths of Figure 1b). The authors performed 7 analyses: each analysis differs for the number of steps imposed: in analysis i (i=1,7), i steps were imposed. At the end of the load-consolidation steps (points i_c, with i=1,7 of Figure 13a) the foundation is further loaded under undrained conditions until ultimate load factor Q_L is reached (points i_f, with i=1,7 of Figure 14a). The numerical results for analysis 7 (the other results are hereafter omitted of the sake of brevity) are plotted in the Q-q plane in Figure 14b.

The displacements accumulated during all the consolidation phases

$$q_d = \sum_{j=1}^{i} \Delta q_{d,j}, \qquad 34.$$

being $\Delta q_{d,j}$ the displacement accumulated during a single consolidation phase, are plotted versus the corresponding Q_L–Q_{Lu} values in Figure 14c. The slope of the interpolating straight line (Equation 33) gives the value of β_d of Table 3.

Finally, η is calibrated on the numerical results corresponding to the partially drained test PD_{18} of Table 2 (Figure 15).

3.2 Validation of the constitutive law

To validate the constitutive relationship, 7 numerical analyses of Table 2 (PD_1, PD_{20} and PD_{21}) and 4 additional tests (PD_{24}-PD_{27} of Table 4) were employed. All these tests are characterized by a constant stress rate (stress paths OB of Figure 1.

	B (m)	σ_{sf0} (kPa)	M (-)	κ (-)	κ/λ (-)	k (m/s)	γ' (kN/m^3)	υ (kPa/day)	t_l (day)	Final σ_{sf} value (kPa)	T_l (-)
PD_{24}	2	20	0.77	0.05	0.4	10^{-8}	10	60	0.53	32	0.008
PD_{25}	2	20	0.77	0.05	0.4	10^{-8}	10	12	3.3	40	0.055
PD_{26}	2	20	0.77	0.025	0.4	10^{-8}	10	6	6.8	41	0.11
PD_{27}	2	20	0.77	0.025	0.4	10^{-8}	10	0.012	20000	240	390

Tab 4: Geometrical/mechanical/hydraulic parameters adopted in the FEM analyses for the constitutive law validation (ν=0.3, e_0=0.5)

In Figures 16 and 17, the FEM numerical results are compared with the model predictions: The constitutive parameters employed are those of Table 3, whereas, as already mentioned, Q_{Lu} is calculated according to Equation 9. As is evident, the agreement is very satisfactory.

3.3 Influence of the loading history on the system response

In this section, the proposed generalized constitutive relationship is employed to put in evidence the influence of loading rate on (i) the limit load and (ii) the accumulation of displacements after the end of the loading process.

The two curves of Figure 18a, obtained by employing the constitutive model, and the points, obtained by performing FEM numerical analyses (geometry and mechanical properties are those of PD_2, PD_{14} and PD_{15} of Table 2 and cases PD_{24}-PD_{26} of Table 4), describe the dependence of the non-dimensional limit load factor (Q_L) on T_l.

It is evident that the curves in the Q_L-T_l plane are characterized by an upward concavity and by a vertical asymptote: the dashed domain of Figure 18a is a sort of partially drained stability domain.

From a practical point of view, both FEM numerical results (symbols of Figure 18a) and the constitutive model predictions (solid and dashed lines of Figure 18a) may be interpolated by using the following expression (Figure 18b):

$$Q_L = Q_{Lu} + \frac{aT_l}{(b-T_l)^c} \qquad 35.$$

where Q_{Lu} is calculated by using Equation 9 whereas a, b and c are non-dimensional interpolating parameters, whose values are reported in Table 5.

a	b	c
10	9.5	0.5

Tab 5: Interpolating parameters for Equation 35

Figure 18 may be fruitfully employed as a design tool according to ultimate limit state approaches (§4.1). Nevertheless, it is worth mentioning that the accumulated displacements under partially drained conditions corresponding to $Q=Q_L$ for T_l larger than 10^{-1} are very often unacceptable.

To emphasise the role of T_l on the accumulation of irreversible displacements, in Figure 19 the theoretical model predictions corresponding to three different loading histories of OAB type (Figure 1) are discussed. In particular, in Figure 19a the results plotted in the Q-q plane correspond to the initial loading phase (OA of Figure 1), whereas in Figure 19b the vertical non-dimensional displacement is plotted against the time period T-T_l corresponding to the consolidation phase (AB of Figure 1).

As is evident, accumulated displacements markedly depend on T_l (final values of the curves of Figure 19a and initial values of the curves of Figure 19b). The same can be observed even at the end of the consolidation phase. This justifies the use of the constitutive relationship to assess how the loading time history affects the final settlements.

4. Practical employment

As it was previously mentioned, the approach proposed by the authors is based on the following assumptions:

- the rigid strip foundation is positioned on a horizontal normally consolidated clayey soil stratum;
- only vertical centred loads are applied on the foundation;
- the loading history is monotonic;
- the foundation "configurational features" (Pisanò et al., 2016), such as the value of the lateral surcharge, footing embedment and underground phreatic level, do not change.

The practical employment of the constitutive relationship may be summarized as it follows (Figure 20):

1) definition of geometry, soil hydraulic/mechanical properties, that is of the 10 input "micro" parameters (Table 6 and Figure 20). **As was previously mentioned (§2.3), the numerical results were obtained by considering a circular cross section for the Modified Cam Clay yield function. Since a plane strain problem is considered, the M value to be employed is not the one derived from experimental standard triaxial compression tests, but this must be reduced to take into consideration the actual shape of the soil failure envelope in the deviatoric plane (e.g Kirkgard & Lade, 1993).**

2) assignment of the loading time history:

$$\sigma_{sf} = \bar{\sigma}_{sf} f(t), \qquad 36.$$

where function $f(t)$ ($0 \leq f(t) \leq 1$) describes the evolution with time of the load;

3a) transformation, by means of Equations 1a and 5, of the dimensional load history into the corresponding non-dimensional one:

$$Q = \bar{Q}F(T), \quad 37.$$

where $\bar{Q}$ is the Q value corresponding to $\bar{\sigma}_{sf}$ (Equation 1a), whereas $F(T)$ is the non-dimensional time function corresponding to $f(t)$;

3b) assessment, by means of Equation 9, of the the undrained non-dimensional bearing capacity Q_{Lu}. This is the unique, owing to the non-dimensional definition of the constitutive model, macro constitutive model parameter depending on geometry/soil properties

The subsequent steps depend on the approach chosen to analyse the problem: the case of ultimate limit state design (ULS) is described in §4.1, whereas the case of displacement based design (DBD) in §4.2.

Geometry	Soil properties		
B, H, σ_{sf0}	γ’	M, λ, κ, ν, e_0	k

Table 6: Micro input parameters

4.1 Ultimate limit state design

In this case, the designer is interested in evaluating the foundation bearing capacity. As was previously emphasised, when partially drained conditions are accounted for, the foundation bearing capacity is not only a function of (i) soil strength and (ii) foundation dimensions, but also of (iii) the soil deformability (Figure 5 and Equation 5), (iv) soil hydraulic properties and (v) imposed loading history.

For the simplest case, in which the load is applied at a constant rate, meaning that

$$F(T) = \frac{T}{T_l}, \quad 38.$$

Equation 35 may be adopted to estimate the non-dimensional foundation bearing capacity (Q_L).

On the contrary, for cases characterised by more complex (but in any case monotonic) loading histories, the bearing capacity cannot be estimated by means of Equation 35. In fact, in case the instantaneous loading rate is significantly larger than the loading rate average value, the foundation failure may take place even for load values lower than the ones estimated by means of Equation 35. Stepwise loading histories are quite common when rapid construction phases are followed by periods during which the load is kept constant. In these cases, by introducing the correct load history in the constitutive relationship (Equation 25) and by integrating this latter, the bearing capacity can be evaluated.

In both cases ($F(T) = T/T_l$ or $F(T) \neq T/T_l$) once the non-dimensional limit load factor Q_L is assessed the dimensional bearing capacity may be calculated by means of Equation 1a.

The dependency of the bearing capacity on soil deformability, permeability and on loading history makes difficult the employment of the current limit state design approaches (e.g. Eurocode 7 CEN, 2004). In fact, as is well known, according to these approaches the partial factors employed in ultimate limit state design only take the variability in the material strength and in the values of the applied loads into account. This topic has been already partially tackled by the authors in Flessati & di Prisco (2020) with reference to tunnel fronts, where an additional partial factor was suggested for soil deformability. An analogous strategy could be followed in this case.

4.2 Displacement based design

After choosing “micro” parameters (Table 6) and the assigned loading time history, the model user will calculate, by means of the constitutive model (Equation 25), the foundation vertical displacement time history (Figure 20) in both non-dimensional (Figure 1b) and dimensional spaces (Figure 1a).

This implies, with a rather negligible computational effort, that the user has the possibility of rapidly assess the scatter of u_{sf} as a function of a predefined variability of (i) soil properties and (ii) load time history.

For the sake of clarity, an exemplifying case is discussed in Appendix 2.

5. Concluding remarks

In this paper a new non-dimensional generalised constitutive relationship, conceived in the framework of the macroelement theory, capable of describing the hydro-mechanical coupled response of shallow foundations resting on clayey soil strata is presented. To achieve this goal, the authors employed a standard upscaling procedure intended to dramatically reduce the computational costs related to the numerical solution of a boundary value problem.

The basic assumption of this constitutive relationship is the presence of two different plastic mechanisms totally activated or partially activated according to the imposed loading rate. One plastic mechanism, governing the response for large loading rates, is characterized by the definition of a failure condition, whereas the other one, governing the response for low loading rates, is characterized by an unlimited hardening response, corresponding to the activation of a punching mechanism progressively involving deeper parts of the spatial domain.

To conceive and calibrate the model, the authors performed a series of hydro-mechanical coupled 2D non-linear FEM numerical analyses in which the soil mechanical behaviour is modelled by means of a strain hardening elastic plastic constitutive relationship. The numerical analyses results were aimed at (i) defining a convenient set of non-dimensional variables and (ii) defining the upscaling procedure putting in relation “micro” to “macro” constitutive parameters.

The proposed generalized constitutive model is characterized by eight macro constitutive parameters. Seven of them are computed once and for all by employing the previously cited upscaling procedure, only one of them has to be calculated. To this goal, an equation based on the FEM numerical data is provided by the authors.

It is worth mentioning that, by considering a different constitutive relationship to reproduce the soil response, the main ingredients of this upscaled model remains unaltered.

Finally, the comparison between the model predictions and numerical FEM data has allowed to appreciate the remarkable predictive capability of the proposed constitutive relationship.

Appendix 1

To obtain Equation 25:

(i) Equations 17 and 22 are substituted into Equation 10:

$$dq = \begin{cases} \frac{1}{K_u^{el}}\mathrm{dQ} + \frac{1}{\alpha_u}\frac{Q_L}{Q_L - Q}\mathrm{dQ} - \mathrm{dQ}' + \frac{\exp\left(\frac{Q'}{\alpha_d}\right)}{K_d^{ep}}\mathrm{dQ}' & \mathrm{dQ} > \mathrm{dQ}' \\ \frac{1}{K_u^{el}}\mathrm{dQ} + \frac{\exp\left(\frac{Q'}{\alpha_d}\right)}{K_d^{ep}}\mathrm{dQ}' & \mathrm{dQ} < \mathrm{dQ}' \end{cases}, \qquad 39.$$

(ii) Equation 21 is integrated and introduced into Equation 15:

$$Q_L = Q_{Lu} + \beta_d \left[\frac{\alpha_d}{K_d^{ep}} \exp\left(\frac{Q'}{\alpha_d}\right) - \frac{Q'}{K_d^{el}}\right] \qquad 40.$$

(iii) Equation 11 is introduced in both Equations 39 and 40:

$$dq = \begin{cases} \left(\frac{1}{K_u^{el}} + \frac{1}{\alpha_u}\frac{Q_L}{Q_L - Q}\right) dQ + \left[\frac{\exp\left(\frac{Q-U}{\alpha_d}\right)}{K_d^{ep}} - \frac{1}{\alpha_u}\frac{Q_L}{Q_L - Q}\right](dQ - dU) & \mathrm{dQ} > \mathrm{dQ'} \\ \frac{1}{K_u^{el}}\mathrm{dQ} + \frac{\exp\left(\frac{\mathrm{Q-U}}{\alpha_d}\right)}{K_d^{ep}}(dQ - dU) & \mathrm{dQ} < \mathrm{dQ'} \end{cases} \tag{41.}$$

$$Q_L = Q_{Lu} + \beta_d \left[\frac{\alpha_d}{K_d^{ep}} \exp\left(\frac{\mathrm{Q-U}}{\alpha_d}\right) - \frac{\mathrm{Q-U}}{K_d^{el}}\right] \tag{42.}$$

(iii) Equation 24 is substituted into Equation 41:

$$dq = \begin{cases} \left(\frac{1}{K_u^{el}} + \frac{1}{\alpha_u}\frac{Q_L}{Q_L - Q}\right) dQ + \left[\frac{\exp\left(\frac{Q-U}{\alpha_d}\right)}{K_d^{ep}} - \frac{1}{\alpha_u}\frac{Q_L}{Q_L - Q}\right]\frac{K_d^{ep}}{\exp\left(\frac{Q-U}{\alpha_d}\right)}\frac{U}{\eta}dT & \mathrm{dQ} > \mathrm{dQ'} \\ \frac{1}{K_u^{el}}\mathrm{dQ} + \frac{\exp\left(\frac{\mathrm{Q-U}}{\alpha_d}\right)}{K_d^{ep}}\frac{K_d^{ep}}{\exp\left(\frac{Q-U}{\alpha_d}\right)}\frac{U}{\eta}dT & \mathrm{dQ} < \mathrm{dQ'} \end{cases} \tag{43.}$$

(iii) Equation 42 is combined with Equation 43.

Appendix 2

Hereafter the model is employed as a preliminary design/monitoring data interpretation tool in relation to the construction of a railway, consisting of a concrete slab track of width B=2.3m (Figure 22). The infrastructure is laid on a clayey soil stratum, 10m thick and resting on a rigid stratum, whose mechanical (that is Modified Cam Clay model parameters) and hydraulic properties are enlisted in Table 7. The concrete base (Figure 22) is founded at a depth of 35cm and, for the sake of simplicity, the water table level is assumed to be coincident with the foundation plane.

M **(-)**	***κ*** **(-)**	***λ*** **(-)**	***e0*** **(-)**	***ν*** **(-)**	γ_{sat} **(kN/m³)**	***k*** ***(m/s)***
1	**0.05**	**0.25**	**0.5**	**0.3**	**20.6**	**$2 \cdot 10^{-8}$**

Table 7: material mechanical/hydraulic properties (the M value is estimated to take into consideration the plane strain conditions)

Once geometry and previously mentioned soil hydraulic/mechanical properties are assigned, we have also derived: $\sigma_{sf0}=\gamma_{sat}D$=7.2kPa, k_0 (Roscoe & Burland, 1968):

$$k_0 = \frac{3+\frac{3}{2}\left(1-\frac{\kappa}{\lambda}\right)-\frac{1}{2}\sqrt{9\left(1-\frac{\kappa}{\lambda}\right)^2+4M^2}}{3-3\left(1-\frac{\kappa}{\lambda}\right)+\sqrt{9\left(1-\frac{\kappa}{\lambda}\right)^2+4M^2}} = 0.71, \qquad 44.$$

S_u=4.5kPa (Equation 3), E_u=657kPa (Equation 4), E=569kPa (Equation 7), c_{v2}=1.12·10^{-6} m^2/s (Equation 6), N_γ*=0.77 (Figure 6a), N_q*=2.56 (Figure 6b), q_{lim}=25 kPa (Equation 9) and $u_{sf,el}$=0.07m (Equation 2), whereas Q_{Lu}=4.58 (Equation 9).

The slab track is composed by three elements (Jang et al., 2008): (i) a cast concrete base, (ii) a precast concrete slab and (iii) the rails, as is sketched in Figure 22.

The construction procedure is expected to consist of three different stages: 1. Soil excavation and the concrete base cast corresponding to the application of an increase in σ_{sf} $\Delta\sigma_{sf,1}=\gamma_c D_b-\gamma_{sat}D$=1kPa (being the concrete unit weight γ_c=25kN/m^3, whereas D_b is the concrete base thickness, as shown in Figure 22), 2. the concrete slab installation corresponding to $\Delta\sigma_{sf,2}=\gamma_c D_s$=4kPa, ($D_s$ is the concrete slab thickness, as shown in Figure 22), 3 the rail installation corresponding to $\Delta\sigma_{sf,3}$=0.7kPa (the rail unit weight is assumed equal to 0.6kN/m) .

All the stages are assumed to last 1 day (T_l=0.02, Equation 5), whereas stage 2 is assumed to begin 9 months (corresponding to a non-dimensional time period ΔT=5) later and analogously stage 3 after other 9 months (Figure 23a).

The chosen load time history is plotted in Figures 23a. By employing Equations 1a and 5, the load time history is converted in its non-dimensional form (the corresponding curve is omitted for the sake of brevity), to be used as input datum in the generalized constitutive relationship (Equation 25). The output in the non-dimensional displacement versus the non-dimensional time plane is then converted in the dimensional results of Figure 23b by using Equations 1b and 5.

From a practical point of view, the displacement time curves can be employed not only in the foundation design phase (for instance, in this case to limit displacements an enlargement of the concrete base could be suggested) but also to interpret monitoring data during the evolution of time and to verify the design assumptions.

List of notation

A vector relating the response variable (dq) and the controlled variables (**X**)
a interpolating parameter for Eq. 35
B foundation width
b interpolating parameter for Eq. 35
C dissipation term of Eq. 22
c interpolating parameter for Eq. 35
c_{v2} 2D consolidation coefficient
D depth of the foundation plane
D_b concrete base thickness
D_s concrete slab thickness
E, E_u drained and undrained Young modulus
e_0 intial void ratio
f_d, f_u drained and undrained yield function
g_d, g_u drained and undrained plastic potential
H soil stratum thickness
I_w non dimensional coefficient for elastic displacements (Giroud, 1972)
J_2 the second invariant of the stress deviator
K_d^{el}, K_u^{el} drained and undrained elastic stiffness (Table 3)
K_d^{el} model parameter (Table 3)
k permeability
$\bar{k}$ geostatic stress anisotropy
M slope of the critical state line
N_q^* , N_γ^* bearing capacity factors
p_0' geostatic average effective stress at a depth equal to B/2
Q non-dimensional stress variable
Q' non-dimensional stress on the drained elastic spring and plastic slider
$\bar{Q}$ final imposed value of Q
Q_d drained hardening variable
Q_{d0} initial value of the drained hardening variable
Q_L internal variable
Q_{Lu} undrained non-dimensional ultimate load factor
$Q_{Lu,FEM}$, $Q_{Lu,th}$ undrained non-dimensional ultimate load factors obtained in numerical analyses and by employing Equation 9
Q_u undrained hardening variable
Q_{u0} intial value of the undrained hardening variable
q non-dimensional strain variable
q_d, q_d^{el}, q_d^{pl} total, elastic and plastic drained non-dimensional strains
q_{lim} foundation bearing capacity
q_u, q_u^{el}, q_u^{pl} total, elastic and plastic undrained non-dimensional strains
S_u undrained strength
T non-dimensional time
T_l non-dimensional loading time
t time
t_l loading time
U non-dimensional stress on the viscous damper
u_{sf} average foundation displacement
$u_{sf,el}$ elastic foundation displacement for $\sigma_{sf}=q_{lim}$

X vector of the controlled variables
α_d, α_u model parameters (Table 3)
β_d model parameter (Table 3)
γ', γ_{sat}, γ_w submerged, saturated soil unit weight and water unit weight
γ_c concrete unit weight
$\Delta\sigma_{sf}$ imposed increment in σ_{sf}
η model parameter (Table 3)
κ unloading reloading line inclination
λ virgin loading line inclination
ν, ν_u Drained and undrained Poisson ratio
σ_{sf} stress applied on the foundation
$\bar{\sigma}_{sf}$ final value of σ_{sf}
σ_{sf0} lateral surcharge
υ loading rate

Figure captions

Fig. 1: definition of a) the dimensional and b) the non-dimensional spaces defining the foundation response
Fig. 2: geometry and spatial discretization
Fig. 3: a) numerical results of Table 1 in the non-dimensional *Q*-*q* plane and b) influence of $\bar{k}$ on the system response
Fig. 4: Numerical results obtained for a constant non-dimensional loading time ($T_l = 0.16$)
Fig. 5: Influence of soil properties/geometry and initial state of stress on the undrained foundation response in the non-dimensional *Q*-*q* plane for cases PD_5-PD_{17} of Table 2 $T_l < 0.024$)
Fig. 6: a) Variation of N_q^* and with the constitutive parameters, b) variation of N_γ^* with the constitutive parameters and c) comparison between the numerical results and the results of Equation 9
Fig. 7: Influence of the loading rate (cases PD_1, PD_5-PD_6, PD_{18}-PD_{23} of Table 2)
Fig. 8: Vertical (a, b), horizontal (c, d) and deviatoric (e, f) strain fields referred to undrained and drained cases, respectively (Points P and R of Figure 7)
Fig. 9 Evolution of obliquity with Q for different points in the domain
Fig. 10: Contour of obliquity (Point R of Figure 7)
Fig. 11: Ground surface displacement profile: a) undrained case (corresponding to point P of Figure 7b) and b) drained case (corresponding to point R of Figure 7a)
Fig. 12: Rheological model
Fig. 13: a) Rheological model for the undrained case and b) comparison between the numerical results and the model predictions (case PD_6 of Table 2)
Fig. 14: a) Rheological model for the drained case and b) comparison between the numerical results and the model predictions (case PD_{23} of Table 2)
Fig. 15: a) definition of the loading-consolidation phases, b) numerical results in the *Q*-*q* plane and c) variation of limit load with the accumulated drained displacements
Fig. 16: Calibration of η on the FEM results (case PD_{18} of Table 2)
Fig. 17: Validation of the generalized constitutive relationship (cases PD_1, PD_{20} and PD_{21} of Table 2)
Fig. 18: Validation of the generalized constitutive relationship (cases PD_{24}-PD_{27} of Table 4)
Fig. 19: Variation of the non-dimensional limit load with the non-dimensional loading time
Fig. 20: a) Foundation response during loading and b) displacement accumulation after the foundation loading
Fig. 21: Practical application of the constitutive relationship
Fig. 22: Sketch of the concrete slab track
Fig. 23: a) imposed stress time history and b) evolution of displacements in time

References

Bienen, B., Byrne, B. W., Houlsby, G. T., & Cassidy, M. J. (2006). Investigating six-degree-of-freedom loading of shallow foundations on sand. Géotechnique, 56(6) 367-379

Butterfield, R. (1980). A simple analysis of the load capacity of rigid footings on granular materials. Journée de Géotechnique, ENTPE, Lyon, France, pp. 128-137.

Carter, J. P., Booker, J. Y., & Yeung, S. K. (1986). Cavity expansion in cohesive frictional soils. Géotechnique, 36(3), 349-358.

Cassidy, M. J., Byrne, B. W., & Randolph, M. F. (2004). A comparison of the combined load behaviour of spudcan and caisson foundations on soft normally consolidated clay. Géotechnique, 54(2), 91-106.

Cassidy, M. J., Randolph, M. F., & Byrne, B. W. (2006). A plasticity model describing caisson behaviour in clay. Applied Ocean Research, 28(5), 345-358.

CEN (2004). EN 1997-1: Geotechnical design: part 1: general rules. Brussels, Belgium: Comité Européen de Normalization

Davis, E. H. & Booker, J. R. (1973). The effect of increasing strength with depth on the bearing capacity of clays. Géotechnique 23, No. 4, 551–563

di Prisco, C. & Flessati, L. (2020) A generalized constitutive relationship for undrained soil structure interaction problems 16th International Conference of the International Association for Computer Methods and Advances in Geomechanics 1-4 July Torino

di Prisco, C., Flessati, L., Cassani, G., Perlo, R. (2019) Influence of the excavation rate on the mechanical response of deep tunnel fronts in cohesive soils. Tunnels and Underground Cities: Engineering and Innovation meet Archaeology, Architecture and Art- Proceedings of the WTC 2019 ITA-AITES World Tunnel Congress, pp. 3654-3663. DOI: 10.1201/9780429424441-387

di Prisco, C., Flessati, L., Frigerio, G. and Lunardi, P. (2018). A numerical exercise for the definition under undrained conditions of the deep tunnel front characteristic curve. Acta Geotechnica, 13, 635-650

di Prisco, C., Flessati, L., Porta, D. (2020) Deep tunnel fronts in cohesive soils under undrained conditions: a displacement-based approach for the design of fibreglass reinforcements Acta Geotechnica, 15 (4), pp. 1013-1030. DOI: 10.1007/s11440-019-00840-8

Flessati, L. & di Prisco, C. (2018) Numerical investigation on the influence of the excavation rate on the mechanical response of deep tunnel fronts in cohesive soils. Springer Series in Geomechanics and Geoengineering, (216849), pp. 1140-1143. DOI: 10.1007/978-3-319-97115-5_55

Flessati, L. & di Prisco, C. (2020) Deep tunnel faces in cohesive soils under undrained conditions: application of a new design approach, European Journal of Environmental and Civil Engineering, In press https://doi.org/10.1080/19648189.2020.1785332

Fu, D., Gaudin, C., Tian, C., Bienen, B., & Cassidy, M. J. (2015). Effects of preloading with consolidation on undrained bearing capacity of skirted circular footings. Géotechnique, 65(3), 231-246.

Giroud, J. P. (1972). Settlement of rectangular foundation on soil layer. Journal of the soil mechanics and foundations division, 98(1), 149-154.

Gottardi, G., Houlsby, G. T., & Butterfield, R. (1999). Plastic response of circular footings on sand under general planar loading. Géotechnique, 49(4), 453-470.

Gourvenec, S. M., Vulpe, C., & Murthy T. G. (2014). A method for predicting the consolidated undrained bearing capacity of shallow foundations. Géotechnique, 64(3), 215-225.

Grange, S., Kotronis, P., & Mazars, J. (2008). A macro-element for a circular foundation to simulate 3D soil–structure interaction. International Journal for Numerical and Analytical Methods in Geomechanics, 32(10), 1205-1227.

Grange, S., Kotronis, P., & Mazars, J. (2009). A macro-element to simulate dynamic soil-structure interaction. Engineering Structures, 31(12), 3034-3046.Grange et al. (2009)

Grange, S., Botrugno, L., Kotronis, P., & Tamagnini, C. (2011). The effects of soil–structure interaction on a reinforced concrete viaduct. Earthquake Engineering & Structural Dynamics, 40(1), 93-105.

Houlsby, G. T., & Cassidy, M. J. (2002). A plasticity model for the behaviour of footings on sand under combined loading. Géotechnique, 52(2), 117-129.

Jang, S. Y., Kang, Y. S., Lee, H. S., Kim, Y. B., & Lee, J. S. (2008). Trial Installation and Performance Evaluation of Prefabricated Concrete Slab Track on Revenue Line. In Proceedings of the KSR Conference (pp. 840-845). Korean Society for Railway.

Kirkgard, M. M., & Lade, P. V. (1993). Anisotropic three-dimensional behavior of a normally consolidated clay. Canadian Geotechnical Journal, 30(5), 848-858.

Martin, C. M., & Houlsby, G. T. (2001). Combined loading of spudcan foundations on clay: numerical modelling. Géotechnique, 51(8), 687-699.

Montrasio, L., & Nova, R. (1997). Settlements of shallow foundations on sand: geometrical effects. Géotechnique, 47(1), 49-60.

Nova, R., & Montrasio, L. (1991). Settlements of shallow foundations on sand. Géotechnique, 41(2), 243-256.

Pisanò, F., Flessati, L., & di Prisco, C. (2016). A macroelement framework for shallow foundations including changes in configuration. Géotechnique, 66(11), 910-926.

Roscoe, K., & Burland, J. B. 1968. On the generalized stress-strain behaviour of wet clay. In Engineering plasticity, pp. 535-609. Cambridge, UK: Cambridge University Press

Salciarini, D., & Tamagnini, C. (2009). A hypoplastic macroelement model for shallow foundations under monotonic and cyclic loads. Acta Geotechnica, 4(3), 163-176.

Salciarini, D., Bienen, B., & Tamagnini, C. (2011). A hypoplastic macroelement for shallow foundations subject to six-dimensional loading paths. In Proc. International Symposium on Computational Geomechanics (ComGeo II), Cavtat-Dubrovnik, Croatia.

Tamagnini, C., Salciarini, D., & Ragni, R. (2013). Implementation of 6–dof hypoplastic macroelement in a finite element code. In Proceeding of the International Conference on Computational Geomechanics (Comgeo III), Krakow.

Viggiani, C. (1967). Sulle condizioni iniziali del processo di consolidazione in un mezzo elastico poroso-saturo. Rivista Italiana di Geotecnica, 3 167-181

Vlahos, G., Cassidy, M. J., & Martin, C. M. (2011). Numerical simulation of pushover tests on a model jack-up platform on clay. Géotechnique, 61(11), 947.

Williams, M. S., Thompson, R. S., & Houlsby, G. T. (1998). Non-linear dynamic analysis of offshore jack-up units. Computers & structures, 69(2), 171-180.

Zdravković, L., Potts, D. M., & Jackson, C. (2003). Numerical study of the effect of preloading on undrained bearing capacity. International Journal of Geomechanics, 3(1), 1-10.

Zhang, Y., Cassidy, M. J., & Bienen, B. (2014). A plasticity model for spudcan foundations in soft clay. Canadian Geotechnical Journal, 51(6), 629-646.

Figure 1

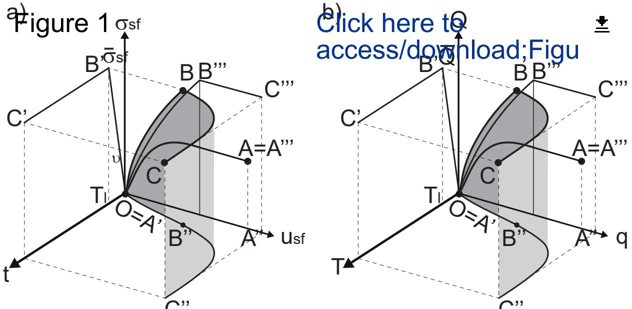

Figure 2

Click here to access/download;Figure;

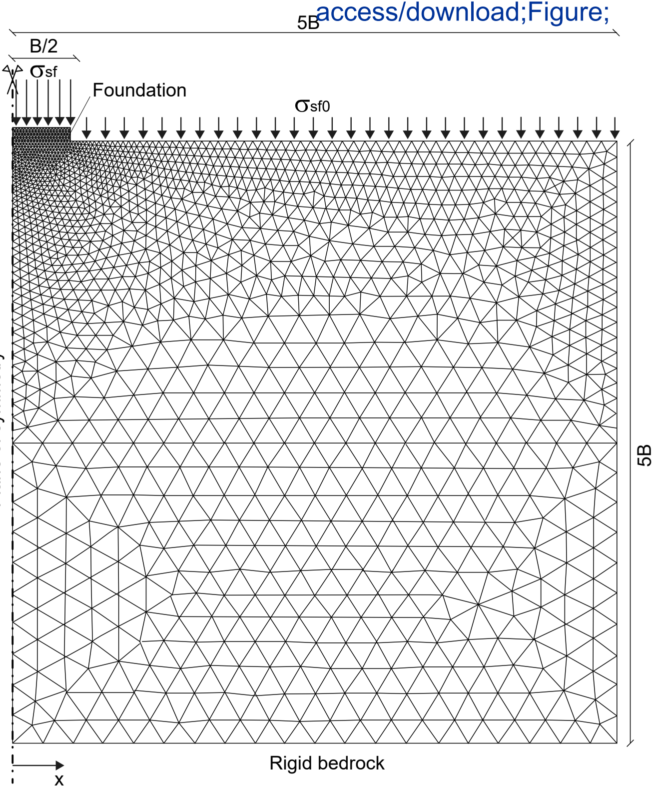

Figure 3

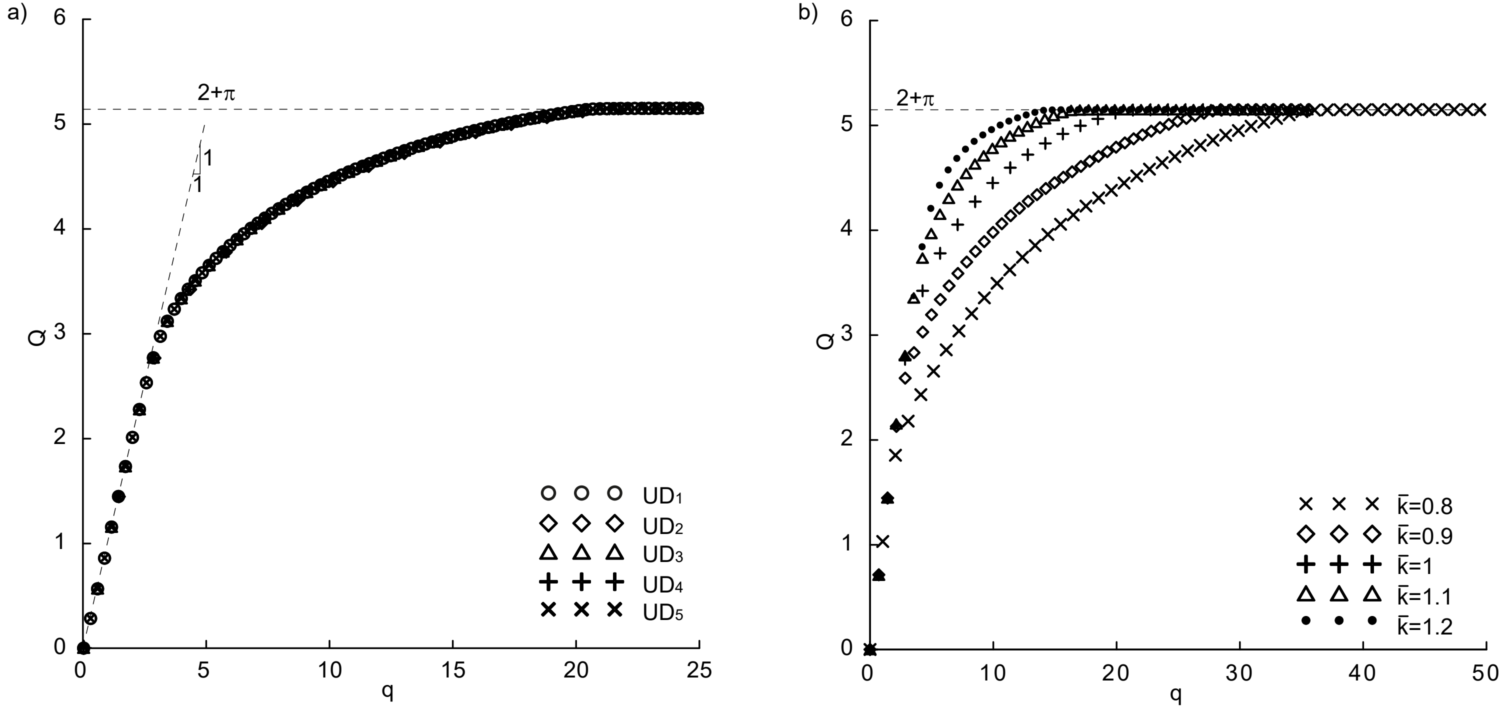
a)
2+π
1
1
Q
q
0
1
2
3
4
5
6
0
5
10
15
20
25
UD1
UD2
UD3
UD4
UD5
b)
2+π
Q
q
0
10
20
30
40
50
k̄=0.8
k̄=0.9
k̄=1
k̄=1.1
k̄=1.2

Figure 4

Click here to access/download;Figure;f

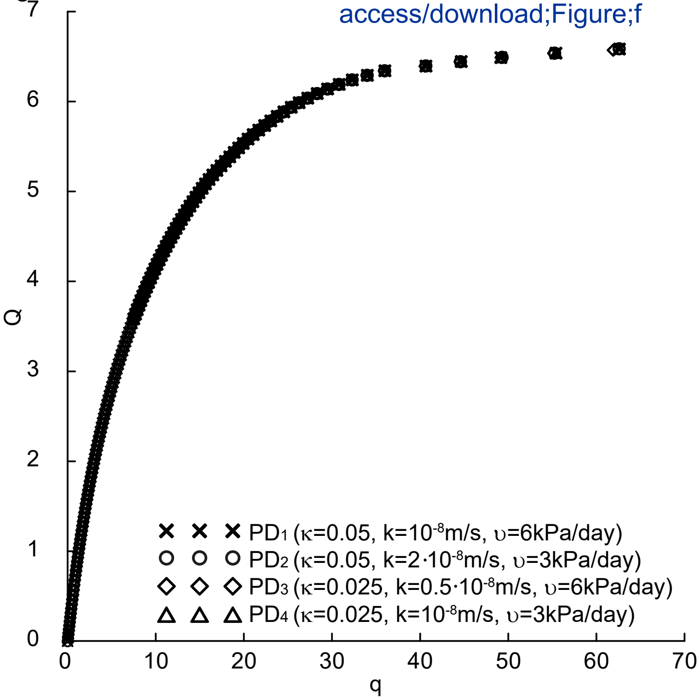

Figure 5

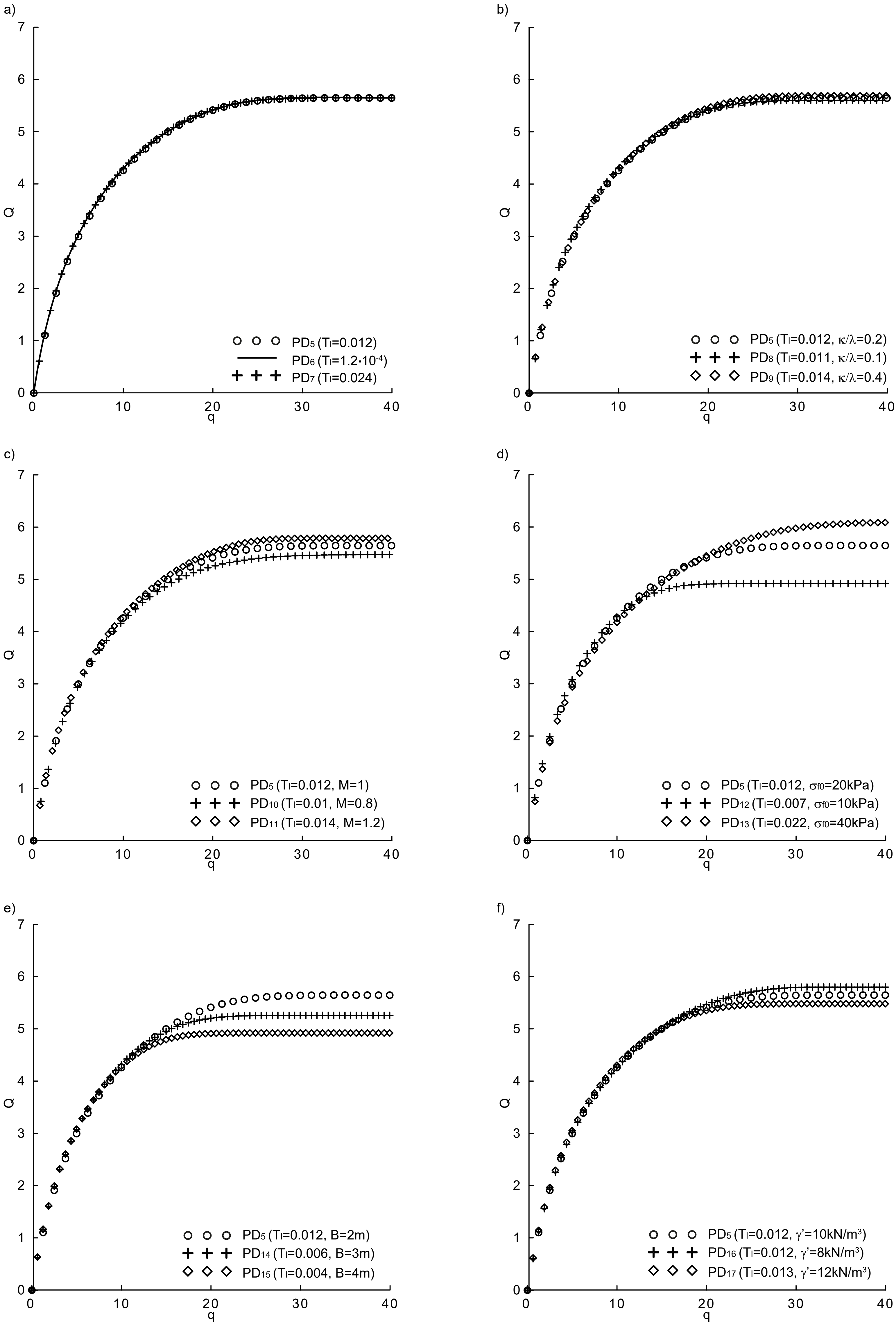
a)
Q
q
PD5 (Tl=0.012)
PD6 (Tl=1.2·10-4)
PD7 (Tl=0.024)
b)
Q
q
PD5 (Tl=0.012, κ/λ=0.2)
PD8 (Tl=0.011, κ/λ=0.1)
PD9 (Tl=0.014, κ/λ=0.4)
c)
Q
q
PD5 (Tl=0.012, M=1)
PD10 (Tl=0.01, M=0.8)
PD11 (Tl=0.014, M=1.2)
d)
Q
q
PD5 (Tl=0.012, σf0=20kPa)
PD12 (Tl=0.007, σf0=10kPa)
PD13 (Tl=0.022, σf0=40kPa)
e)
Q
q
PD5 (Tl=0.012, B=2m)
PD14 (Tl=0.006, B=3m)
PD15 (Tl=0.004, B=4m)
f)
Q
q
PD5 (Tl=0.012, γ'=10kN/m3)
PD16 (Tl=0.012, γ'=8kN/m3)
PD17 (Tl=0.013, γ'=12kN/m3)

Figure 6

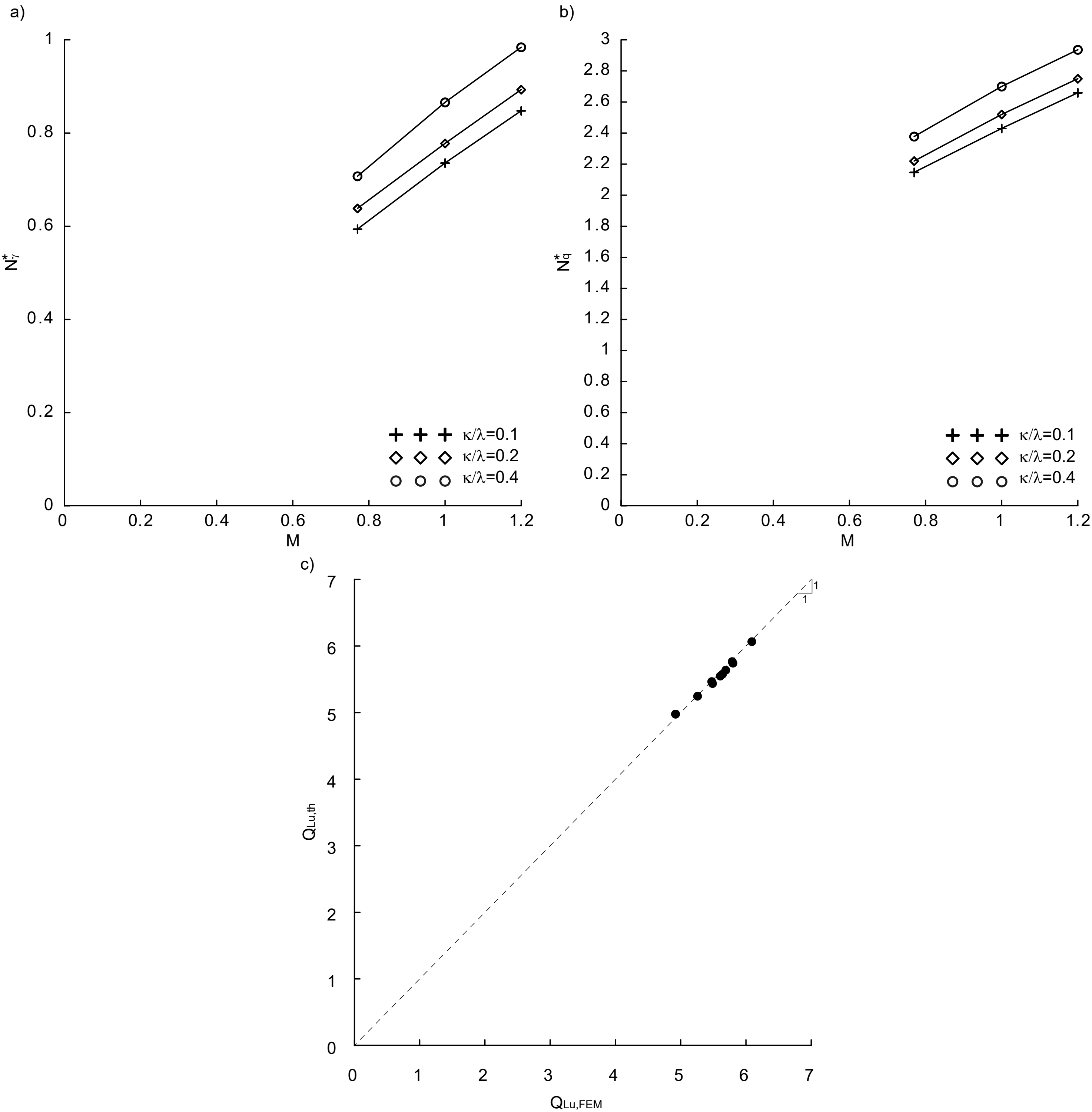

a)
N^*_γ
M
κ/λ=0.1
κ/λ=0.2
κ/λ=0.4
b)
N^*_q
M
κ/λ=0.1
κ/λ=0.2
κ/λ=0.4
c)
$Q_{Lu,th}$
$Q_{Lu,FEM}$
1
1

Figure 7

Click here to access/download;Figure;fig7.pdf

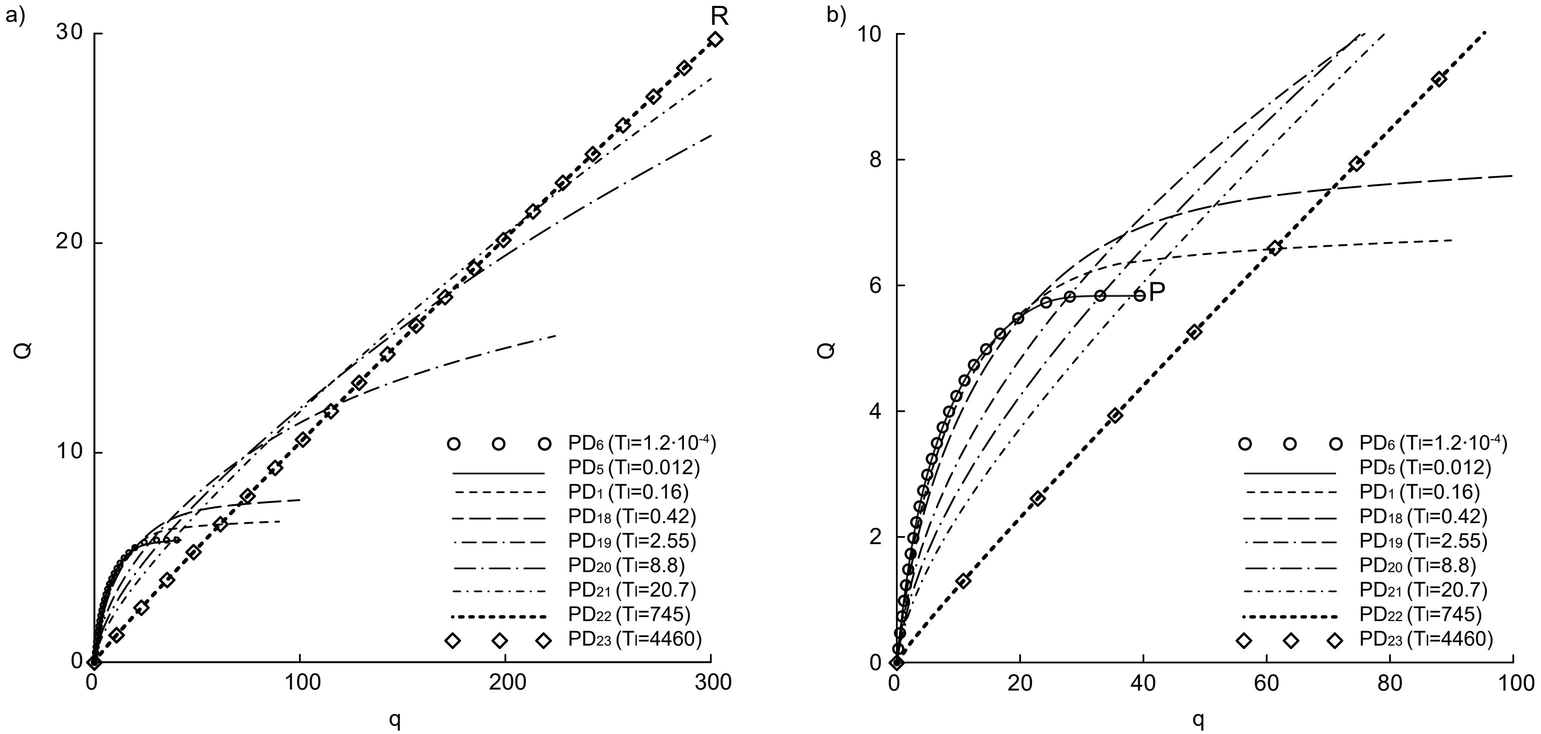

Figure 8

Click here to access/download;Figure;fig8.pdf

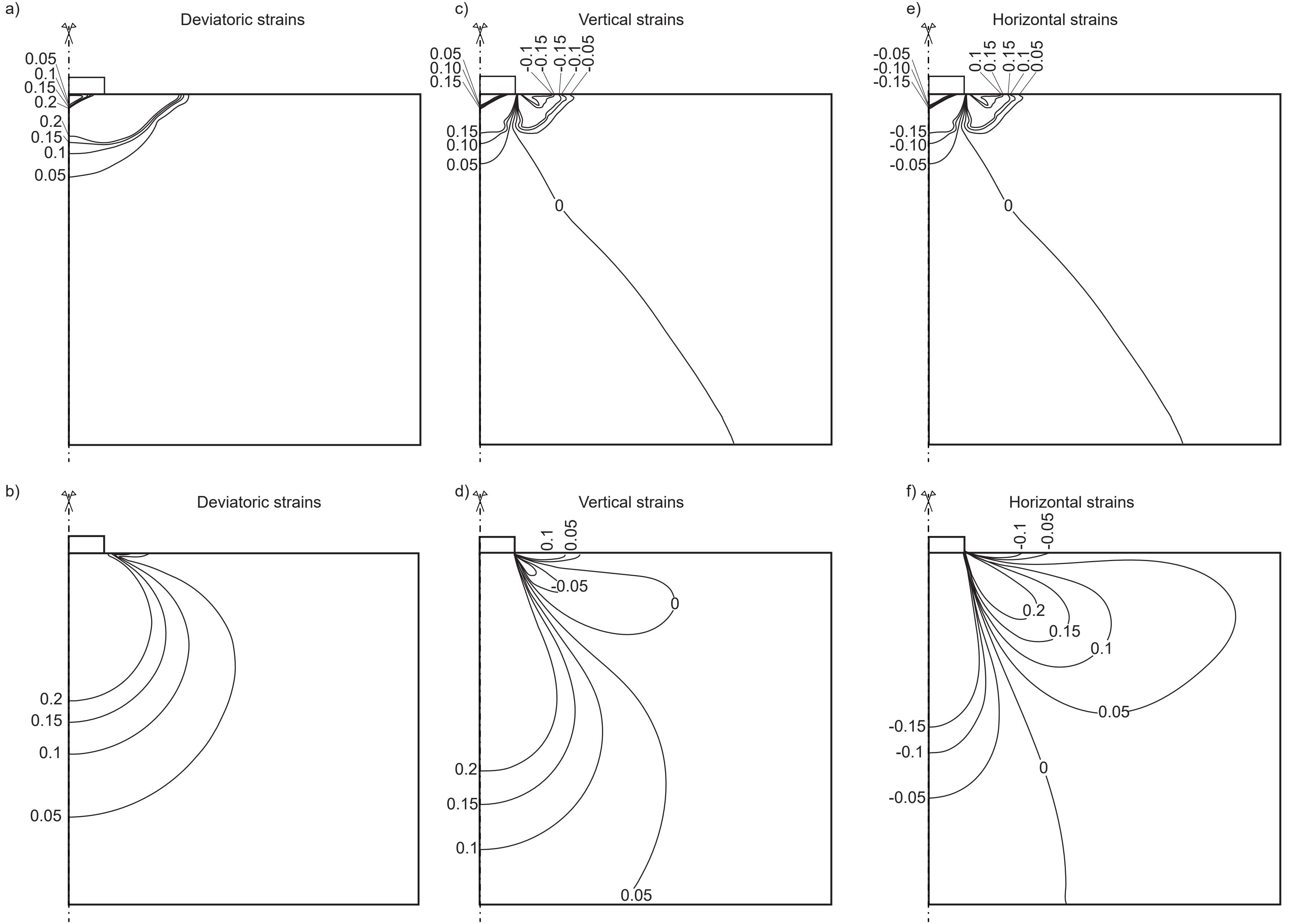

Figure 9

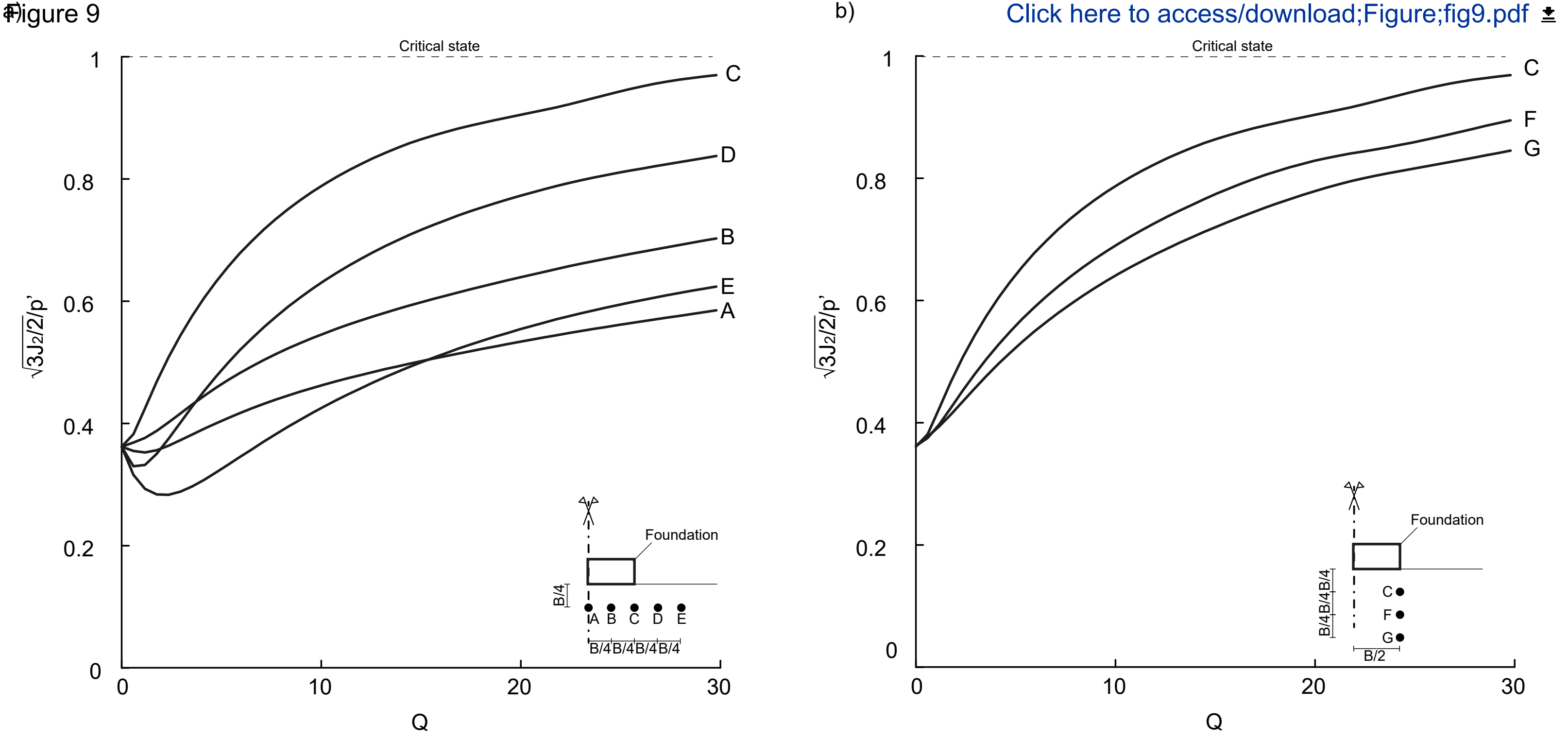
a)
Critical state
1
0.8
0.6
0.4
0.2
0
√3J2/2/p'
C
D
B
E
A
Foundation
B/4
A B C D E
B/4 B/4 B/4 B/4
0
10
20
30
Q
b)
Critical state
C
F
G
Foundation
B/4 B/4 B/4
B/2
Q

Figure 10

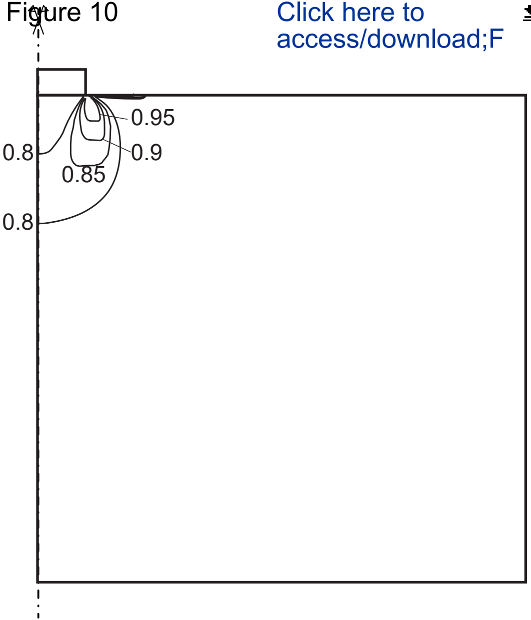

Figure 11

a)

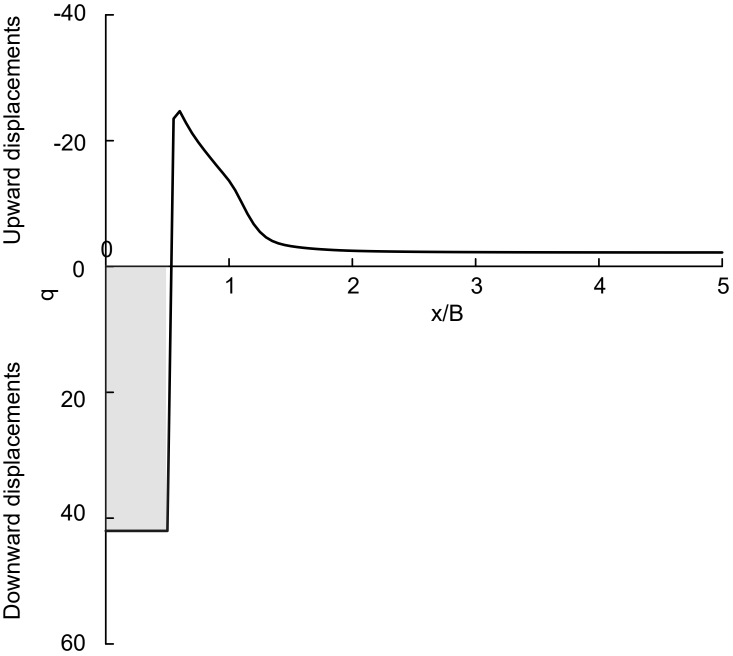
-40
-20
0
20
40
60
Upward displacements
Downward displacements
q
0
1
2
3
4
5
x/B

b)

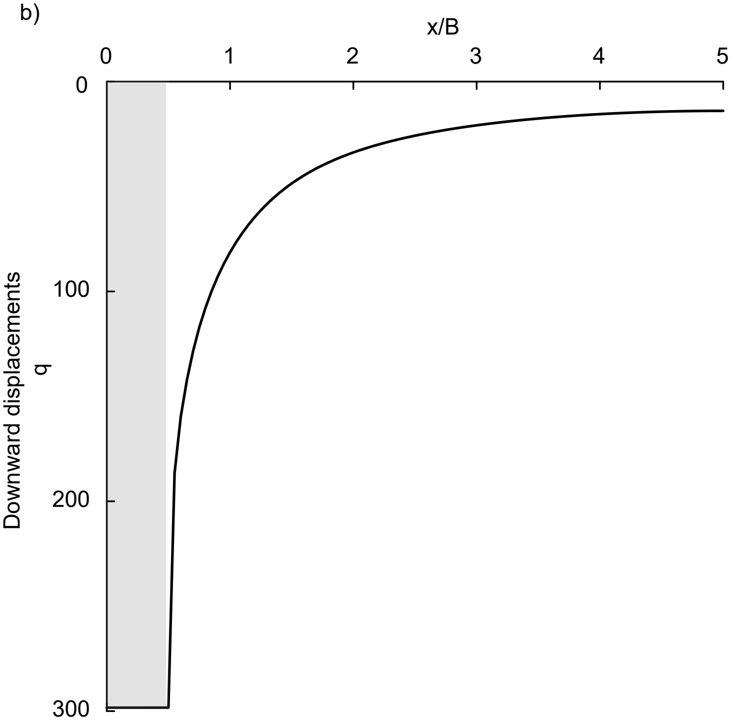
x/B
0
1
2
3
4
5
0
100
200
300
Downward displacements
q

Figure 12

Click here to access/download;Fi

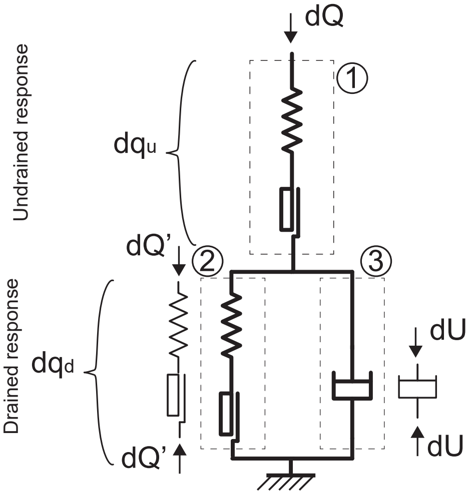

Figure 13

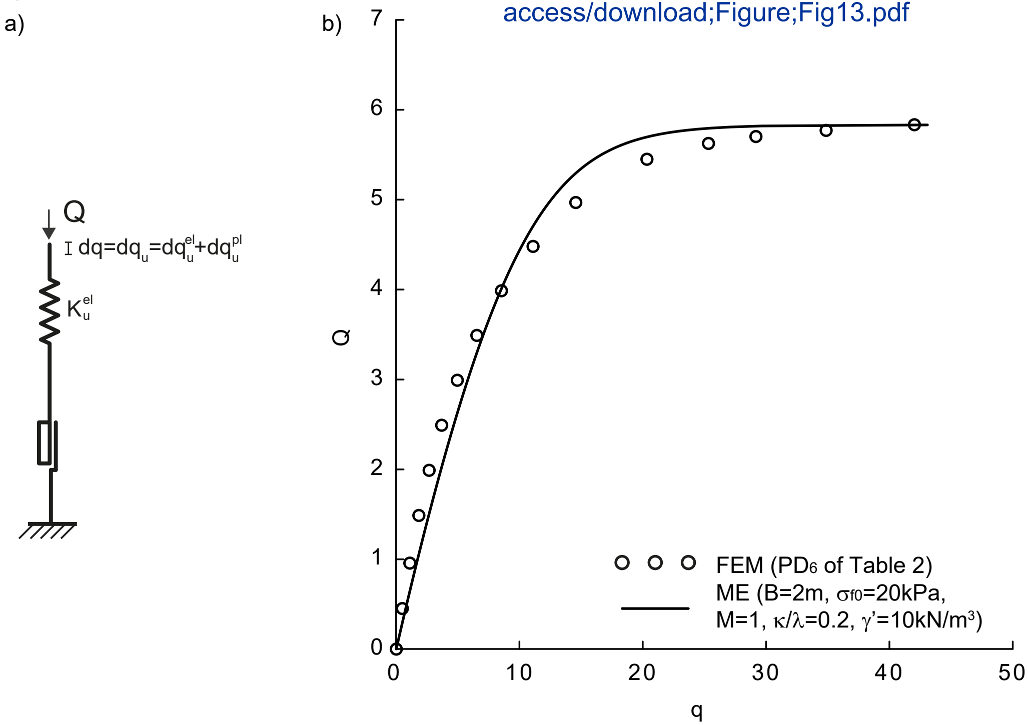
a)
Q
dq=dq_u=dq_u^el+dq_u^pl
K_u^el
b)
Q
q
0
1
2
3
4
5
6
7
0
10
20
30
40
50
FEM (PD6 of Table 2)
ME (B=2m, σf0=20kPa,
M=1, κ/λ=0.2, γ'=10kN/m3)

Figure 14

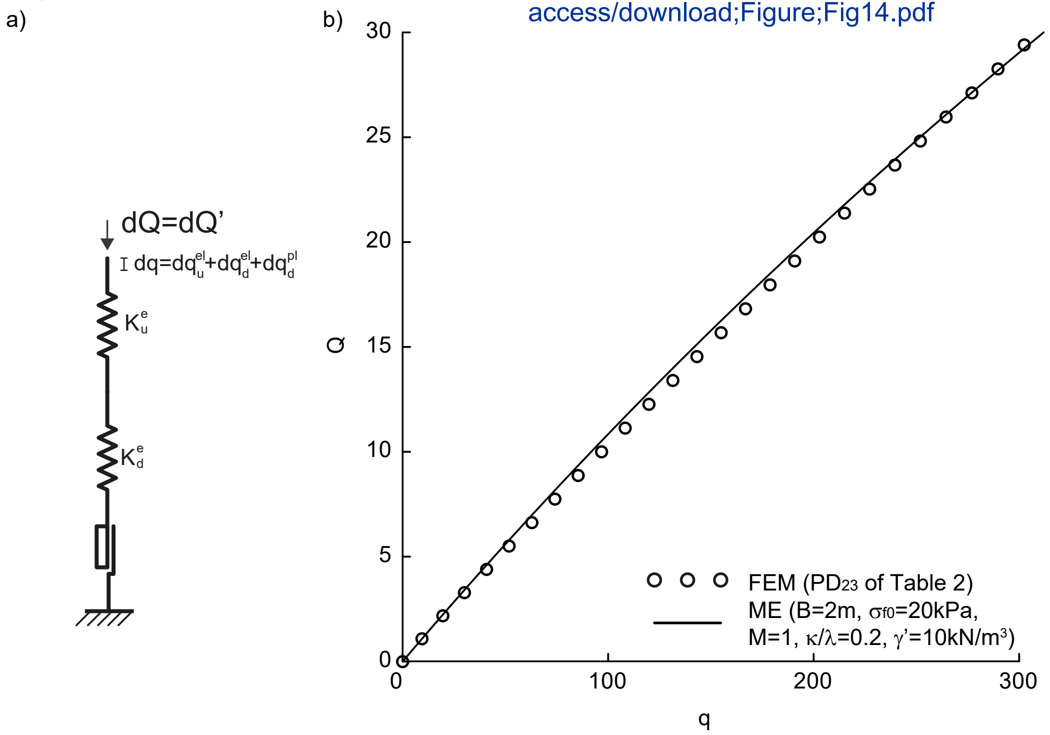

Click here to access/download;Figure;Fig14.pdf

Figure 15

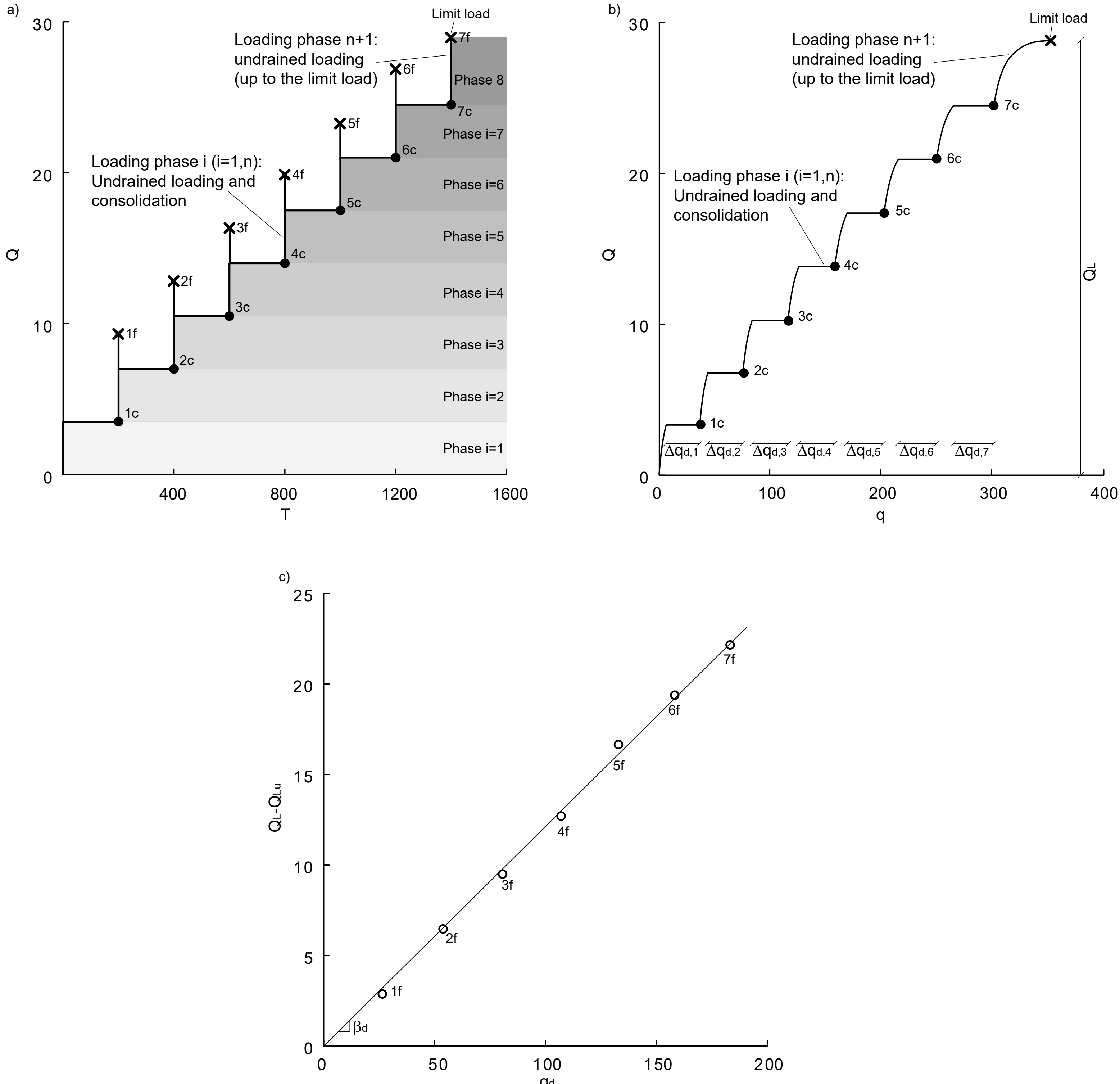
a)
Limit load
Loading phase n+1:
undrained loading
(up to the limit load)
Loading phase i (i=1,n):
Undrained loading and
consolidation
1f
2f
3f
4f
5f
6f
7f
1c
2c
3c
4c
5c
6c
7c
Phase 8
Phase i=7
Phase i=6
Phase i=5
Phase i=4
Phase i=3
Phase i=2
Phase i=1
Q
T
0
10
20
30
400
800
1200
1600
b)
Limit load
Loading phase n+1:
undrained loading
(up to the limit load)
Loading phase i (i=1,n):
Undrained loading and
consolidation
1c
2c
3c
4c
5c
6c
7c
Δqd,1
Δqd,2
Δqd,3
Δqd,4
Δqd,5
Δqd,6
Δqd,7
Q
QL
q
0
10
20
30
0
100
200
300
400
c)
QL-QLu
qd
βd
1f
2f
3f
4f
5f
6f
7f
0
5
10
15
20
25
0
50
100
150
200

Figure 16

Click here to access/download;Figure;fi

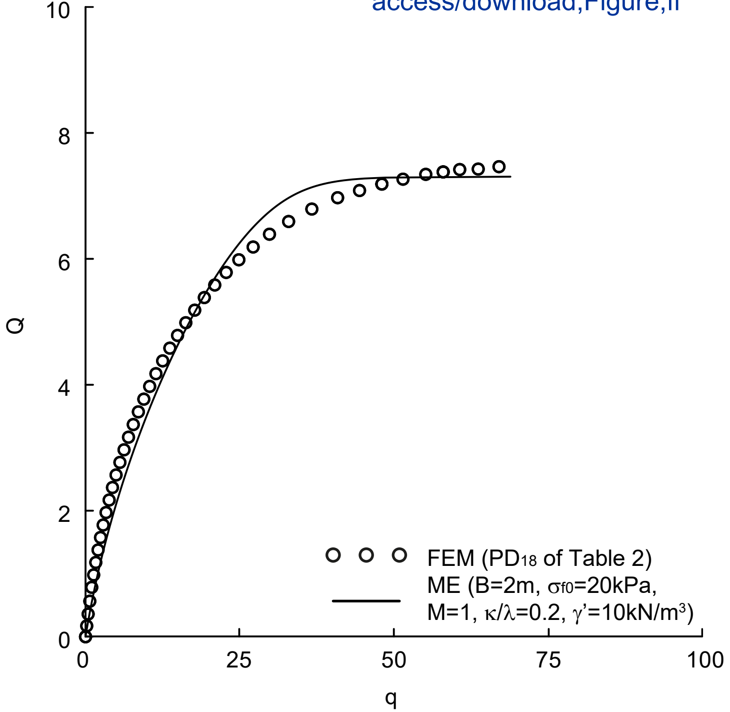

Figure 17

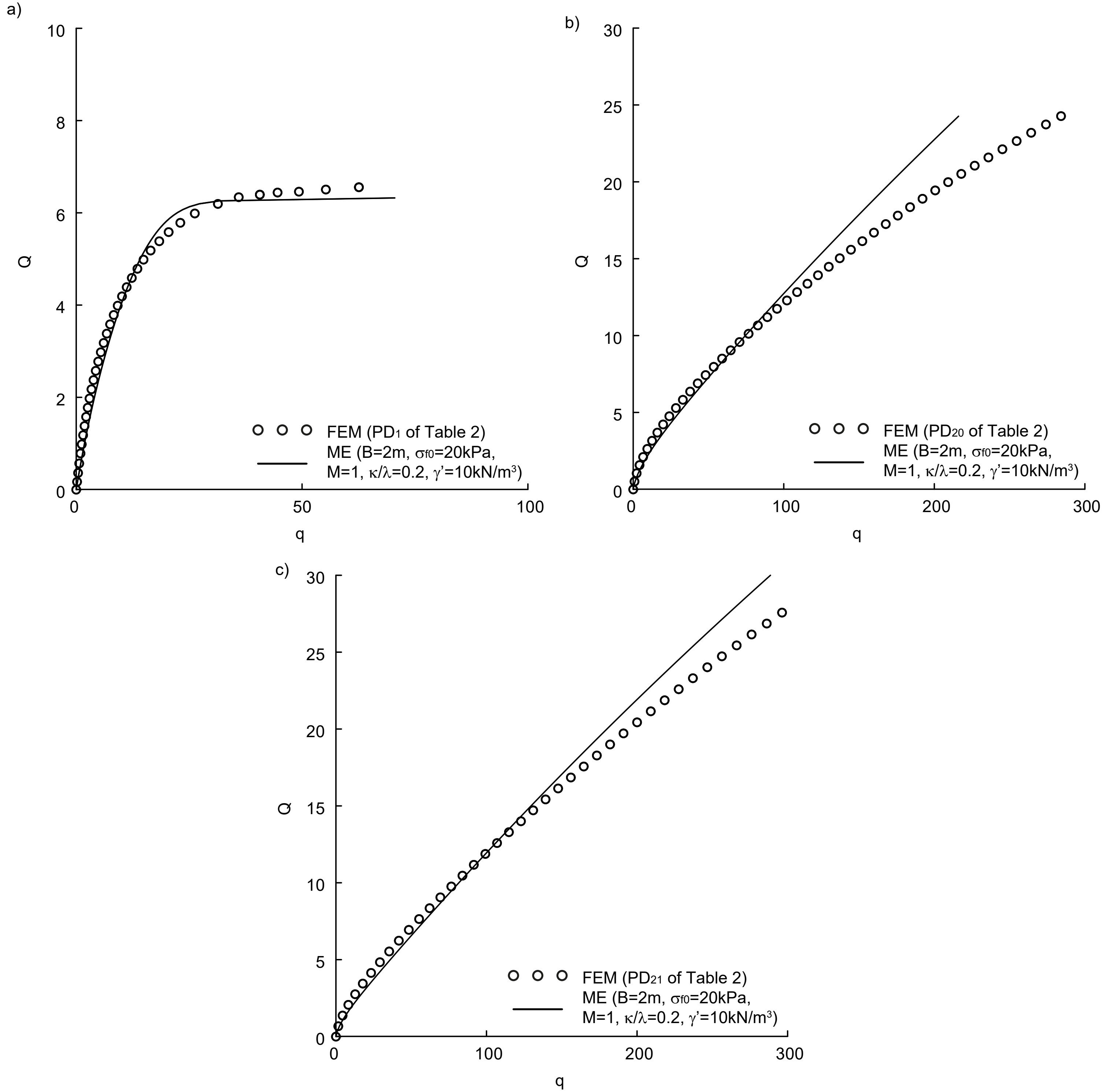
a)
Q
q
0
2
4
6
8
10
0
50
100
FEM (PD1 of Table 2)
ME (B=2m, σf0=20kPa,
M=1, κ/λ=0.2, γ'=10kN/m³)
b)
Q
q
0
5
10
15
20
25
30
0
100
200
300
FEM (PD20 of Table 2)
ME (B=2m, σf0=20kPa,
M=1, κ/λ=0.2, γ'=10kN/m³)
c)
Q
q
0
5
10
15
20
25
30
0
100
200
300
FEM (PD21 of Table 2)
ME (B=2m, σf0=20kPa,
M=1, κ/λ=0.2, γ'=10kN/m³)

Figure 18

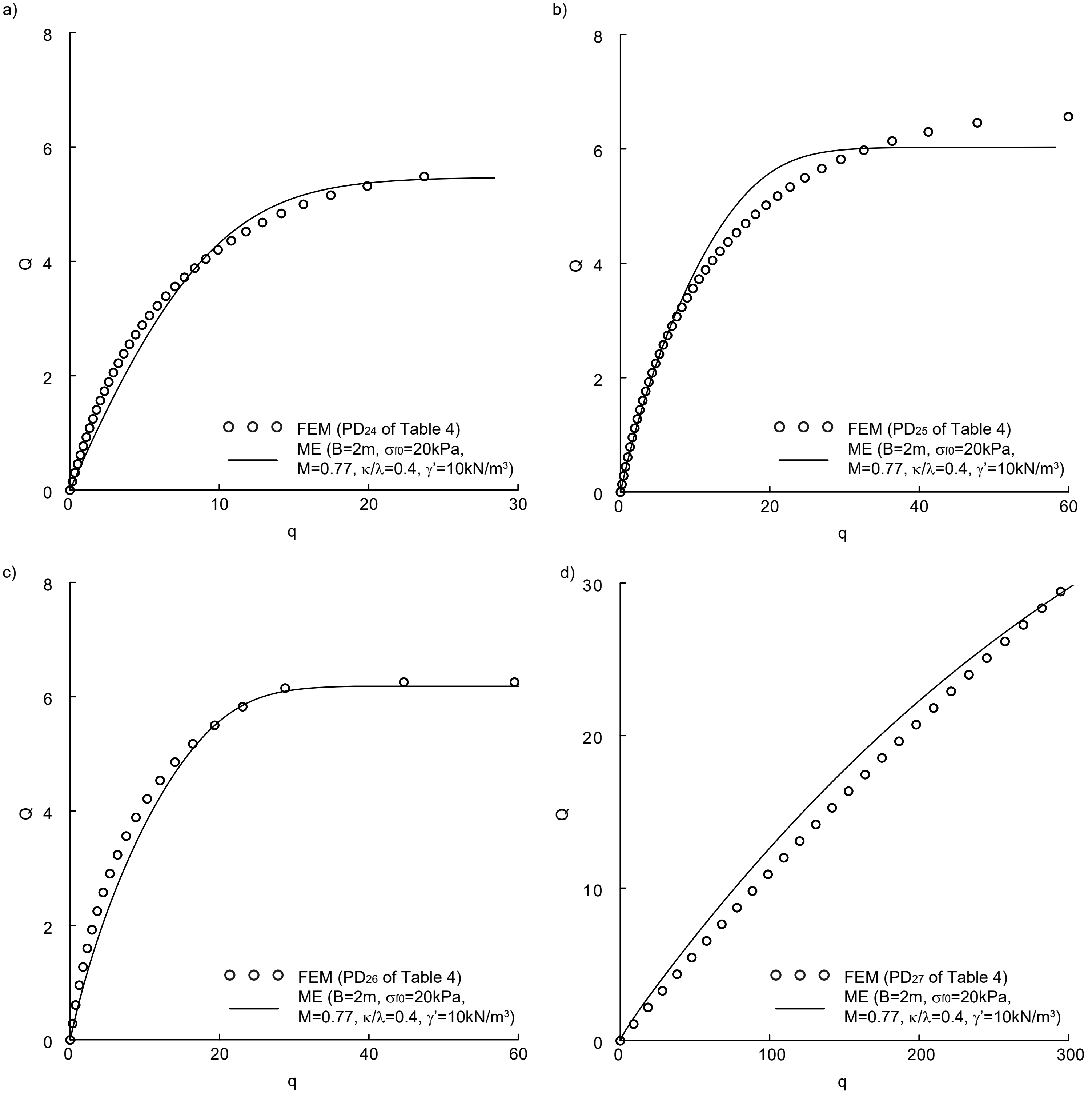
a)
Q
q
FEM (PD24 of Table 4)
ME (B=2m, σf0=20kPa,
M=0.77, κ/λ=0.4, γ'=10kN/m³)
b)
Q
q
FEM (PD25 of Table 4)
ME (B=2m, σf0=20kPa,
M=0.77, κ/λ=0.4, γ'=10kN/m³)
c)
Q
q
FEM (PD26 of Table 4)
ME (B=2m, σf0=20kPa,
M=0.77, κ/λ=0.4, γ'=10kN/m³)
d)
Q
q
FEM (PD27 of Table 4)
ME (B=2m, σf0=20kPa,
M=0.77, κ/λ=0.4, γ'=10kN/m³)

Figure 19

Click here to access/download;Figure;fig19.pdf

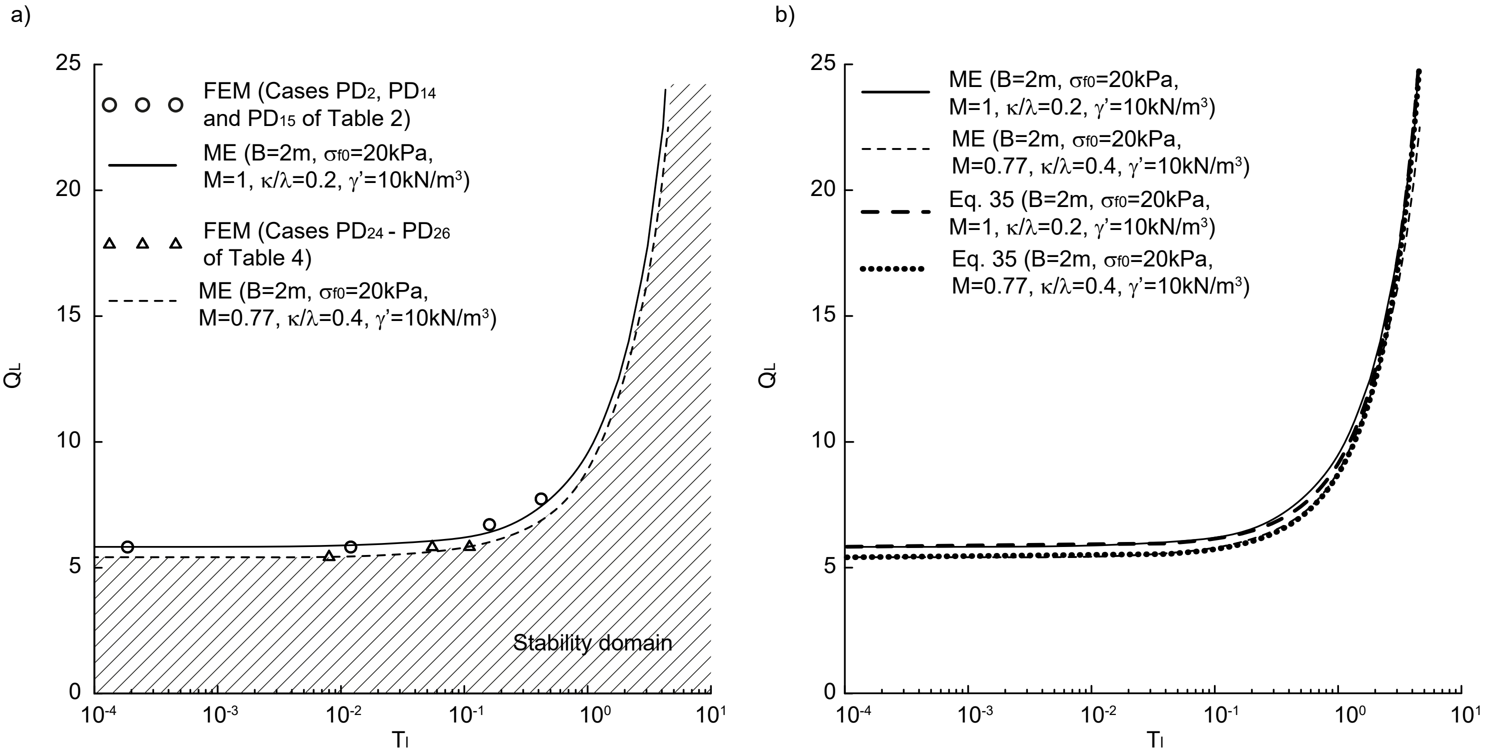

Figure 20

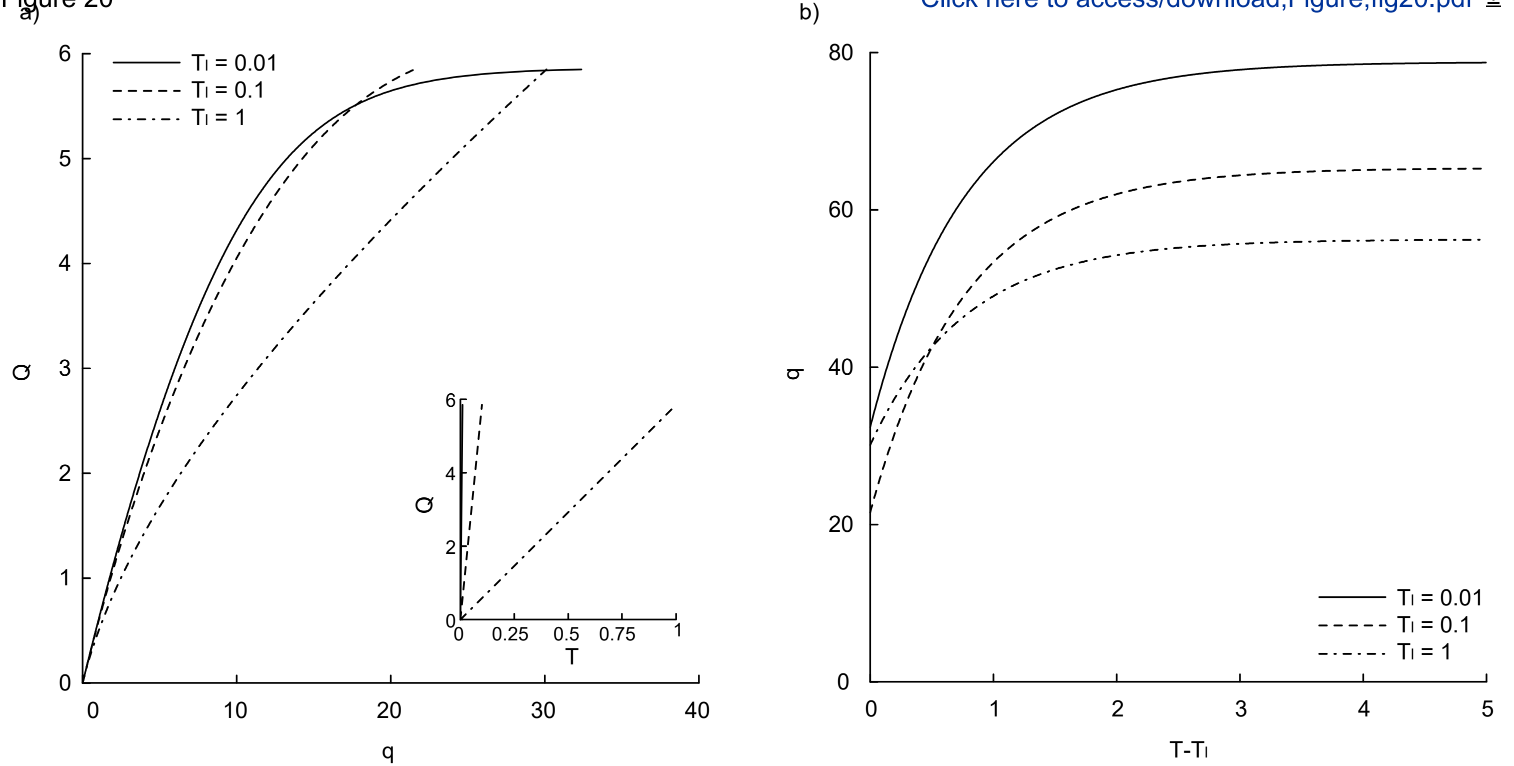
a)
Tl = 0.01
Tl = 0.1
Tl = 1
Q
q
0
1
2
3
4
5
6
0
10
20
30
40
T
0.25
0.5
0.75
b)
q
T-Tl
0
20
40
60
80
0
1
2
3
4
5
Tl = 0.01
Tl = 0.1
Tl = 1

Figure 21

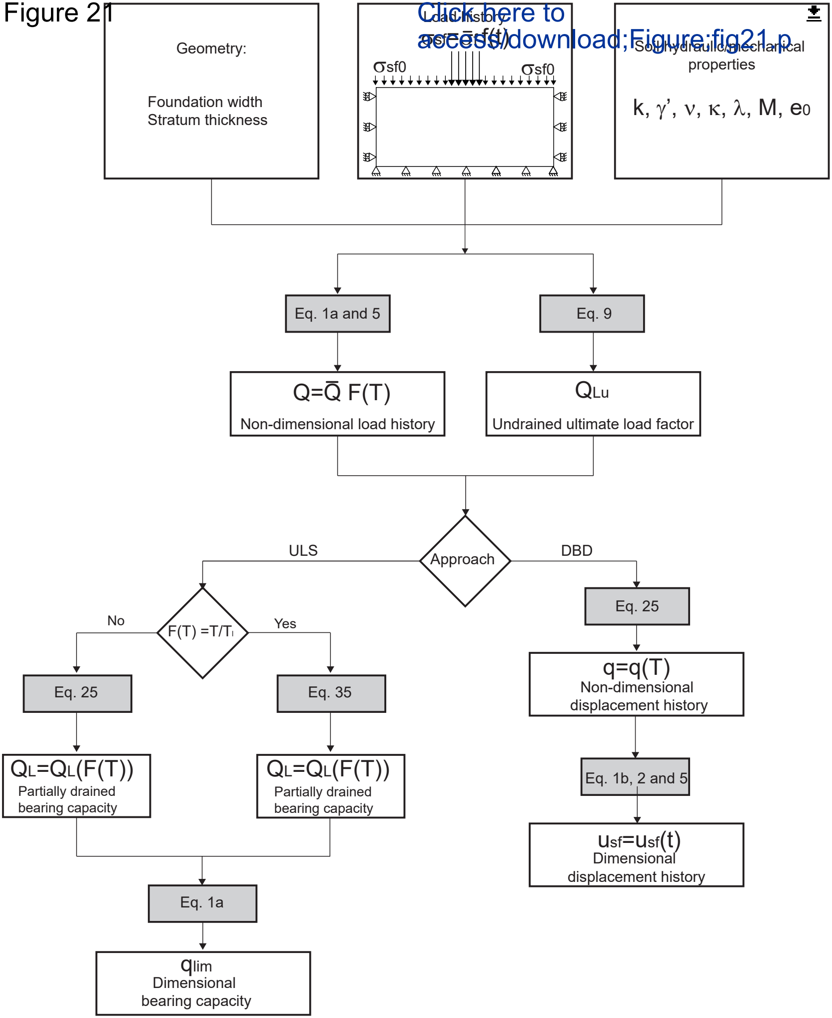
Geometry:
Foundation width
Stratum thickness
Load history
σsf =σsf(t)
σsf0
σsf0
Soil hydraulic/mechanical properties
k, γ', ν, κ, λ, M, e0
Eq. 1a and 5
Eq. 9
Q=Q̄ F(T)
Non-dimensional load history
QLu
Undrained ultimate load factor
Approach
ULS
DBD
F(T) =T/Tl
No
Yes
Eq. 25
Eq. 35
Eq. 25
QL=QL(F(T))
Partially drained bearing capacity
QL=QL(F(T))
Partially drained bearing capacity
q=q(T)
Non-dimensional displacement history
Eq. 1b, 2 and 5
usf=usf(t)
Dimensional displacement history
Eq. 1a
qlim
Dimensional bearing capacity

Figure 22

Click here to access/download;Fi

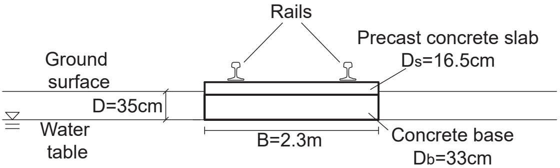

Figure 23

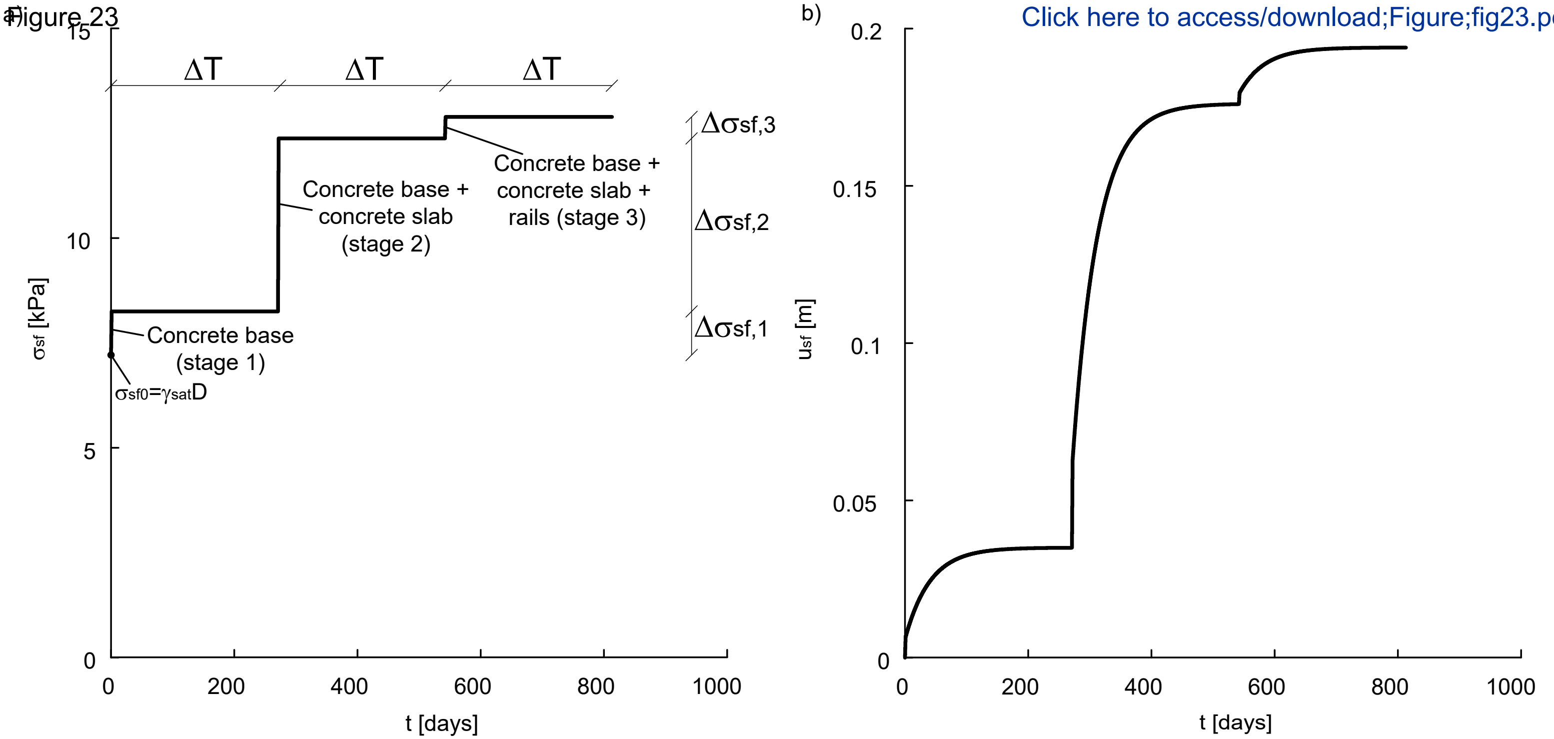
a)
15
10
5
0
0
200
400
600
800
1000
t [days]
σsf [kPa]
ΔT
ΔT
ΔT
Δσsf,3
Δσsf,2
Δσsf,1
Concrete base
(stage 1)
Concrete base +
concrete slab
(stage 2)
Concrete base +
concrete slab +
rails (stage 3)
σsf0=γsatD
b)
0.2
0.15
0.1
0.05
0
0
200
400
600
800
1000
t [days]
usf [m]